MINISTERE DE L'ENSEIGNEMENT SUPERIEUR
ET DE LA RECHERCHE SCIENTIFIQUE

UNIVERSITE FELIX
HOUPHOUËT-BOIGNY

RÉPUBLIQUE DE CÔTE D'IVOIRE
UNION - DISCIPLINE - TRAVAIL

TRAINING AND RESEARCH UNIT
FOR STRUCTURE SCIENCES OF
MATTER AND TECHNOLOGY

Institute of Energy
Technologies (IET-3)

N°: 829

SPONSORED BY THE
Federal Ministry
of Education
and Research

INTERNATIONAL MASTER PROGRAM

IN RENEWABLE ENERGY AND GREEN HYDROGEN

SPECIALITY:

PRODUCTION AND TECHNOLOGY OF GREEN HYDROGEN

MASTER THESIS

Topic:

INVESTIGATION OF ELECTRONIC AND IONIC STRUCTURES OF SELECTED HIGH ENTROPY CHLORIDES FOR APPLICATION AS AN ELECTRODE IN BATTERIES

Presented on September 24, 2025, by:

Mamaja Jalloh

Jury:

Dr(MC) ZAHIRI Eric Pascal	**President**
Professor ELLO Aimé Serge	**Examiner**
Dr. MC. ESSY Kouadio Fodjo	**Supervisor**
Prof. Dr. rer. nat. EIKERLING Michael	**Co-Supervisor**
Dr. KOWALSKI Piotr M.	**Co-Supervisor**

Academic year 2024-2025

DEDICATION

To my parents, with gratitude for their limitless love and support, whose sacrifices made this possible.

To Dr. Piotr M. Kowalski, whose guidance shaped each word of this master's thesis and a mentor who guided me in every step through the process.

To my friends, who always encourage me, never let me quit, even when I wanted to, and give me words of self-confidence and encouragement.

ACKNOWLEDGEMENTS

In the name of Allah, the Entirely Merciful, the Especially Merciful. Alhamdulillah, for the gift of life, good health, strength, courage, patience, and fortitude throughout my life and studies.

I express my sincere gratitude to the Federal Ministry of Education and Research (BMBF) and the West African Science Service Centre on Climate Change and Adapted Land Use (WASCAL) for the opportunity to pursue my masters in this highly competitive area with a fully funded scholarship and networking opportunities.

I want to thank the President of Université Félix Houphouët-Boigny, Professor BALLO Zié, for his generous support in allowing me to do my third semester, my thesis and for awarding the certificate upon program completion. I would also like to thank the President of the University, Abdou Moumouni Professor MAMADOU Saidou, the President of the Université de Lomé, Professor KPODAR Adama Mawule, whose generous hospitality and support were instrumental in the first and second semesters of the program.

I am especially indebted to Professor Michael Eikerling, Director of the IET-3 Institute and my lecturer, whose vision and generosity made it possible for me to visit Germany and work under Dr. Piotr's supervision, whose warm welcome makes my stay at IET-3 a memorable one and the whole research team for the direction, availability, and technical support provided to me while on my research visit.

I would also like to acknowledge Dr ESSY Kouadio Fodjo, my local supervisor, whose constant guidance has been key in bringing my work to the institutional level of quality. His suggestions still inform the final section of my master’s thesis.

I want to express my most profound appreciation to the jury members, Dr. (MC) ZAHIRI Eric Pascal, and Professor ELLO Aimé Serge for sparing their valuable time, carefully considering my master’s thesis, providing valuable insights, and contributing substantially to the achievement of this scholastic work.

My heartfelt appreciation goes to Professor Thomas Tränapp, the Vice Chancellor of RWTH Aachen University, for allowing us to conduct my research in his university and for making the university's facilities open to me.

I would also like to express my deepest gratitude to the Directors of the Graduate Studies Programme (GSP), Togo, Professor Komi AGBOKA, and Niger, Professor Adamou RABANI, for the tremendous amount of academic and administrative support experienced throughout the first and second semesters. Additionally, I would like to further express my

deepest gratitude to the Director of the Graduate Studies Programme (GSP), Côte d'Ivoire, Professor Kouassi Edouard, and the Deputy Director, Professor Souleymane Konate, for the opportunity to study and specialise in their programme and for the great experience both academically and the foreseen opportunities that they had open to us.

Furthermore, I would like to appreciate the coordinator, Dr. Wanignon Ferdinand FASSINOU, and the Scientific Coordinator, Dr. SORHO Fatogoma, for their devotion to seeing the success of running the program throughout my stay in Côte d'Ivoire.

I would also like to extend my heartfelt gratitude to Dr. Piotr M. KOWALSKI, a great mentor. Not only did he co-organise the experimental work with Dr Evgeny V. ALEKSEEV, but he also guided me through the whole writing process, provided continuous mentorship, and opened many doors of opportunity. His assistance went beyond the computational environment, involving proofreading my master's thesis, poster, curriculum vitae, and other papers. His assistance has been the overriding factor of the experience I gathered in Germany.

I also wish to extend my gratitude to Dr. Evgeny V. Alekseev, co-author of the experimental research and the motivating force behind the project on which my master's dissertation was based. His technical expertise and enthusiasm made it a success.

In addition, it is with great pleasure to recognise that Dr. Conor J. Price has always supported my research. He helped me understand complex coding, walked me through the world of scientific knowledge and writing, and provided guidance on both my poster presentation and master's thesis. His time to provide me with the necessary foundation was greatly appreciated.

I also want to thank my classmate-fellow IMP-EGH scholars for the support and friendship, as they make this experience rich and rewarding.

Moreover, I would be indebted and thankful for the everlasting assistance, prayer, and sacrifice by my family, friends, and loved ones. My performance would never have been possible without their assistance and faith in my capability.

This dissertation results from the collective efforts, assistance, and comments that the complete persons and organisations listed above provide. I thank you all from the depths of my heart.

ABSTRACT

The integration, growth, and penetration of renewable energy requires durable, cost-effective, and sophisticated materials for energy storage. Current Lithium-ion batteries (LIBs) are the major players due to their longer cycle life, high energy density, and other advantages; however, their performance is limited by the materials used for the cathodes, namely the common transition oxides. High-entropy materials (HEMs) and high-entropy chlorides (HECls) are promising alternatives due to their entropy stability and optimised transport properties. This work explores electronic and ionic structures of such systems as $Li_2[Me^{2+}]Cl_4$ where Me is Zn, Mn, Co, Mg, and Fe to crown their potential as cathode materials. Density functional theory (DFT) calculations using the Quantum ESPRESSO package were done by including both constant and element-dependent Hubbard *U* corrections to consider the present correlation effects due to transition-metal d-orbitals suitably. From the analysis, the density of states (DOS), band structure, and the spin polarisation in single-component as well as multi-component chlorides were focused on. Binary chlorides such as, $FeCl_4$, $MnCl_4$, and $CoCl_4$ exhibit an insulating nature through intense spin polarisation, while $ZnCl_4$ and $MgCl_4$ are wide-bandgap non-magnetic insulators. Multi-component high-entropy chlorides exhibit a broader electronic-state distribution across the Fermi surface, characterised by d-bands, resulting in a range of semiconductor or insulating properties. The results show that the entropy effect found in high-entropy chlorides results in substantial electronic changes, which can potentially enhance the conductivity and cycling stability of the single-component counterparts. The electronic density of states computed here will facilitate and help to explain the subsequent experimental results (XANES, EXAFS) from Forschungszentrum Jülich colleagues. This work maps out a pathway to developing high-entropy halide cathodes and suggests $Li_2[Me^{2+}]Cl_4$ as potential materials for next-generation rechargeable batteries.

Key words: density of states; high-entropy materials; high-entropy chlorides; density functional theory; electronic structure; *ab initio;* single and multiple phases; lithium-ion batteries.

RÉSUMÉ

L'intégration, la croissance et la pénétration des énergies renouvelables nécessitent des matériaux durables, rentables et sophistiqués pour le stockage de l'énergie. Les batteries lithium-ion (LIB) actuelles sont les principaux acteurs en raison de leur durée de vie plus longue, de leur haute densité énergétique et d'autres avantages ; cependant, leur performance est limitée par les matériaux utilisés pour les cathodes, à savoir les oxydes de transition courants. Les matériaux à haute entropie (HEMs) et les chlorures à haute entropie (HECls) sont des alternatives prometteuses en raison de leur stabilité entropique et de leurs propriétés de transport optimisées. Ce travail explore les structures électroniques et ioniques de tels systèmes que $Li_2[Me^{2+}]Cl_4$ où Me est Zn, Mn, Co, Mg et Fe pour couronner leur potentiel en tant que matériaux de cathode. Les calculs de la théorie fonctionnelle de la densité (DFT) en utilisant le package Quantum ESPRESSO ont été effectués en incluant à la fois des corrections de Hubbard U constantes et dépendantes des éléments pour prendre en compte de manière appropriée les effets de corrélation présents dus aux orbitales d des métaux de transition. À partir de l'analyse, la densité d'états (DOS), la structure de bande et la polarisation de spin dans les chlorures à un composant ainsi qu'à plusieurs composants ont été étudiées. Les chlorures binaires tels que $FeCl_4$, $MnCl_4$ et $CoCl_4$ présentent une nature isolante en raison d'une intense polarisation de spin, tandis que $ZnCl_4$ et $MgCl_4$ sont des isolants non magnétiques à large bande interdite. Les chlorures à haute entropie multicomposants présentent une distribution plus large des états électroniques à travers la surface de Fermi, caractérisée par des bandes d, ce qui entraîne une gamme de propriétés semi-conductrices ou isolantes. Les résultats montrent que l'effet d'entropie trouvé dans les chlorures à haute entropie entraîne des changements électroniques substantiels, ce qui peut potentiellement améliorer la conductivité et la stabilité cyclique des homologues à un seul composant. La densité électronique d'états calculée ici facilitera et aidera à expliquer les résultats expérimentaux ultérieurs (XANES, EXAFS) des collègues du Forschungszentrum Jülich. Ce travail trace une voie vers le développement de cathodes halogénures à haute entropie et suggère $Li_2[Me^{2+}]Cl_4$ comme matériaux potentiels pour les batteries rechargeables de nouvelle génération.

Mots-clés : densité d'états ; matériaux à haute entropie ; chlorures à haute entropie ; théorie de la fonctionnelle de la densité ; structure électronique ; ab initio ; phases simples et multiples ; batteries lithium-ion.

ACRONYMS AND ABBREVIATIONS

Acronym	Definition
An:	Actinides
B3LYP:	Becke, 3-parameter, Lee–Yang–Parr hybrid functional
DFT:	Density Functional Theory
DFT+U:	Density Functional Theory with Hubbard U correction
DOS:	Density of States
EXAFS:	Extended X-ray Absorption Fine Structure
GGA:	Generalized Gradient Approximation
HEAs:	High-Entropy Alloys
HECls:	High-Entropy Chlorides
HEO:	High-Entropy Oxides
HSE:	Heyd-Scuseria-Ernzerhof hybrid functional
LDA:	Local Density Approximation
LIBs:	Lithium-ion Batteries
Ln:	Lanthanides
LT-Mos:	Layered Lithium Transition Metal Oxides
PBE:	Perdew–Burke–Ernzerhof
QE:	Quantum ESPRESSO
RPA:	Random Phase Approximation
Ry:	Rydberg (unit of energy)
SCAN:	Strongly Constrained and Appropriately Normed functional

Acronym	Definition
SCF:	Self-Consistent Field
TM:	Transition Metals
TPSS:	Tao–Perdew–Staroverov–Scuseria functional
WASCAL:	West African Science Service Center on Climate Change and Adapted Land Use
XC:	Exchange–Correlation
XANES:	X-ray Absorption Near Edge Structure

LIST OF TABLES

Table 1: Electronic properties of binary and multi $Li_2[Me^{2+}]Cl_4$ compounds (computed in High Spin) at fixed Hubbard U = 5 eV 41

Table 2 : Electronic properties of binary $Li2[Me2+]Cl4$ compounds (computed in Low Spin) at fixed Hubbard U = 5 eV 43

Table 3: Electronic properties of binary $Li_2[Me^{2+}]Cl_4$ compounds (computed in High Spin) with element-specific Hubbard U values 46

Table 4: Electronic properties of binary $Li_2[Me^{2+}]Cl_4$ compounds (computed in Low Spin) with element-specific Hubbard U values 49

LIST OF FIGURES

Figure 1.1: Schematic diagram of the battery working principle (Meena, 2021)..... 9
Figure 1.2: The lithium-ion battery's components (LIBs) (Aida, 2022)..... 9
Figure. 1.3: The detailed scheme of a lithium-ion battery (Al-Gabalawy et al., 2020)..... 10
Figure 1.4: Electrochemical reactions that occur during charging. 11
..... 11
Figure 1.5: Electrochemical reactions during discharge..... 11
Figure 1.6: Schematic of Goodenough's battery during discharge, with a $LiaCoO2$ cathode. Figure reproduced from the Nobel Prize Website (Wu, 2015)..... 12
Figure 1.7: Ionic diffusion mechanisms via Li-Ion hopping in layered (a, c) and spinel structures (b, d) as modelled by Van Der Ven et al. (Van Der Ven et al., 2013). 18
Figure 1.8: High-entropy effect on a spinel-type structure(Schumacher et al., 2025). 18
Figure: 2. DOSs of penta-graphene, LiC54, LiC3, and LiC1.5. (Xiao et al., 2016)..... 28
Figure 3.1: Single-phase and multi-phase (computed in High Spin) for various plots of the Density of States (DOS) as a function of Energy 40
Figure 3.2: Single-phase and multi-phase (computed in Low Spin) for various plots of the Density of States (DOS) as a function of Energy 43
Figure 3.3: Single-phase and multi-phase (computed in High Spin) for various plots of the Density of States (DOS) as a function of Energy 48
Figure 3.4: Single-phase and multi-phase (computed in Low Spin) for various plots of the Density of States (DOS) as a function of Energy 48

TABLE OF CONTENTS

DEDICATION ..... *ii*

ACKNOWLEDGEMENTS ..... *iii*

ABSTRACT ..... *v*

RÉSUMÉ ..... *vi*

ACRONYMS AND ABBREVIATIONS ..... *vii*

LIST OF TABLES ..... *ix*

LIST OF FIGURES ..... *x*

GENERAL INTRODUCTION *2*

CHAPTER 1: LITERATURE REVIEW *7*

INTRODUCTION **7**

1.1 Batteries: **7**

1.1.1 Battery Working Principle **8**

1.1.2 Components of Lithium-Ion Batteries (LIBs) **9**

1.1.3 Scheme of Lithium-Ion Batteries **10**

1.1.4 Function of Batteries **12**

1.1.5 Electrodes **13**

1.1.6 Conventional Batteries **14**

1.2 High-Entropy Materials (HEMs) **14**

1.3 Four key properties (effects) of High-Entropy Materials **15**

1.4 Interconnection of the Primary Effects **16**

1.5 high-entropy alloys (HEAs) **17**

1.6 High-entropy Oxides (HEOs) **17**

1.7 High-Entropy Chlorides (HECLs) **19**

CONCLUSION **20**

CHAPTER 2: MATERIAL AND METHODS *22*

INTRODUCTION **22**

2.1 ab initio **Density Functional Theory** **22**

2.2 Schrödinger's time-independent Equation **23**

2.3 Density Functional Theory **23**

2.4 X Exchange-Correlation Functional in Density Functional Theory **25**

2.5 Electronic property **27**

2.6 Band structure **27**

2.7 Density of States **28**

2.8 Computational approach **30**

2.8 The Hubbard *U* Parameter **31**

2.9 Quantum ESPRESSO **32**

CONCLUSION **33**

CHAPTER 3: RESULTS AND DISCUSSIONS ***36***

INTRODUCTION **36**

Model 1: U = 5 eV **36**

Model 2: Variable U values **43**

Conclusion **50**

CONCLUSION AND PERSPECTIVES ***52***

Conclusion **52**

Perspectives **53**

BIBLIOGRAPHIC REFERENCES ***54***

GENERAL INTRODUCTION

GENERAL INTRODUCTION

Never-ending search for high-performance materials with properties that align with the specifications of increasingly demanding technological requirements constitutes a daunting challenge for the field of material science (Rost et al., 2015). The most critical part of the energy transition is finding cost-efficient, compact, and durable materials for energy storage (Gallo et al., 2016; Kalair et al., 2021; Koohi-Fayegh & Rosen, 2020). Materials should not only be cost-efficient and compact but must also be durable during the process of energy generation, conversion, and storage (Grey & Tarascon, 2016; Stamenkovic et al., 2016).

Hence, there is a competitive push to discover higher energy and/or power density materials for energy storage devices (Grey & Tarascon, 2016).

Incorporation of renewable energy sources largely relies on the discovery of cost-effective and high-performance materials for energy storage. This objective would be accomplished by taking a whole approach that brings together novelty modelling strategies and experimental methods (Kowalski et al., 2023).

In general, large-scale energy storage is of four types: mechanical, electrical, chemical, and electrochemical (Soloveichik, 2011). The increasing demand for grid-scale energy storage is multidimensional, driven by factors like the capital cost incurred in flattening peak demands, investment cost incurred for grid reliability, and requirements for energizing renewable energy sources The majority of modern energy storage is now controlled by pumped hydroelectric facilities, but battery facilities also seem to have a lot of promising futures, if their costs can be brought down. 99 percent of the 127,000 MW discharge power capacity in the globe is found in pumped hydroelectric projects. With 440 MW, compressed air storage comes in far behind (Dunn et al., 2011).

Electrochemical energy storage generally has a series of desirable attributes, including pollution-free operation, high round-trip efficiency, flexible power and energy features for many grid uses, long cycle life, and low maintenance. Batteries are an excellent energy storage technology for integrating renewable resources. Their compactness guarantees that they are appropriate for scattered locations, and they may provide frequency control to minimise variability of local solar generation and wind farm swings. Although high costs for the time being limit market penetration, the inherent modularity and scalability of different battery systems guarantee reduced cost in the next couple of years (Dunn et al., 2011). Successful electrochemical energy storage and conversion depend on high-performance electrodes, electrolytes, or catalyst materials (Kowalski et al., 2023).

Several rechargeable battery types have been financially successful and widely used (Dehghani-Sanij et al., 2019; Liang et al., 2019; C. Zhang et al., 2018). Currently, lithium-ion batteries (LIBs) are the most advanced rechargeable batteries because of their high power and energy density, good cycle life performance, and acceptable safety performance (Blomgren, 2017; Deng, 2015; Kim et al., 2019). Nevertheless, further improvement of these performance characteristics is still required for the widespread application of LIBs as giant capacity storage devices. One major constraint to LIB capability in capacity and overall cost is the positive electrode (cathode), which in all present-day batteries primarily consists of layered lithium transition metal oxides (LT-MOs), such as, $LiCoO_2$ (LCO) (Fergus, 2010; Julien et al., 2014; Shi et al., 2018). Transition metal oxides are used extensively as cathode materials in rechargeable Li-ion batteries (Ting & Kowalski, 2023). Sustainable substitutes, such as $LiNiO_2$ (LNO), (Ni, Co, Mn)-oxides (NCM), and high entropy disordered-rocksalt (HE-DRX), are being considered as cobalt-based cathode substitutes that are both toxic and expensive (Kalyani & Kalaiselvi, 2005; S. Liu et al., 2014; Lun et al., 2021; Mukai et al., 2010). Compared to the field of electrochemical energy storage systems, high-entropy design thinking has been reported to provide favourable impacts on battery material performance by suppressing undesirable short-range order, slowing down the energy landscape, suppressing volumetric changes, and suppressing primary metal dependence (Ouyang & Zeng, 2024). The current project focuses on the investigation of the ionic and electrical structures of some high-entropy chlorides. Specifically, the electronic structures of Li-chlorides of 3d-elements (including Mg) with $Li_2[Me^{2+}]Cl_4 (Me^+: \mathrm{Fe, Co, Mn, Zn, and\ Mg})$ compositions are investigated. Phase structures of this type are especially of significant interest since they can be employed as cathode-side battery materials.

Identification of novel materials and the follow-up investigation on their structures and properties are central components within materials engineering and science. As long as first-principles grounded atomistic simulation tools are accurate, they can be effectively utilised to pre-screen potential target materials possessing good electronic structure, redox capability, and phase stability, thereby facilitating the identification of novel cathode materials (Zhang et al., 2013). Over the last two decades, atomistic modelling has become very popular in many fields of research, including energy materials (Chroneos et al., 2013; Jahn & Kowalski, 2014; Wu et al., 2019). The development of high-performance computing and computational software has made it possible to study complex systems with hundreds of atoms from first principles (Jahn & Kowalski, 2014). For over thirty years, *ab initio*

calculations like our work have been extensively used for computational research on a large variety of energy materials, particularly those dealing with electrochemistry, energy storage, and nuclear energy production (Kowalski et al., 2023). The results of such research have yielded fruitful information about structural (Beridze et al., 2016; Blanca-Romero et al., 2014; Connor et al., 2021; Feng et al., 2013; Rustad, 2012), electronic (Blanca-Romero et al., 2014; Cui et al., 2022; Kowalski et al., 2021; Kowalski, Beridze, et al., 2017; Lee et al., 2017; Murphy et al., 2021; Tesch & Kowalski, 2022), elastic (Ali et al., 2016; Feng et al., 2013; Ji, Beridze, Bosbach, et al., 2017; Kowalski, Ji, et al., 2017; Kowalski & Li, 2016; J. Wang et al., 2005), thermodynamic (Eremin et al., 2019; Feng et al., 2013; Ji, Beridze, Li, et al., 2017; Kowalski et al., 2015, 2016, 2021; Li et al., 2014; Mogilevsky, 2007; Neumeier et al., 2017), thermochemical parameters (Beridze et al., 2016; Kowalski, 2020; Rustad, 2012), electrochemical interface properties (Krishnamurthy et al., 2004; K. Lee et al., 2017; Tesch et al., 2021), and radiation damage resistance (Cui et al., 2022; Ji, Kowalski, et al., 2017; Jolley et al., 2017; Kowalski & Li, 2016; Li et al., 2016). Energy materials usually incorporate d and f elements (transition metals (TM), lanthanides (Ln), actinides (An)) that play an active role in determining the properties of the material. These elements include strongly correlated electrons, which are difficult to compute by computational quantum chemistry (Vogiatzis et al., 2019). In this context, X-ray spectroscopy (XANES/EXAFS) in combination with molecular-level simulations can efficiently provide significant information regarding the electrical and ionic composition of potential electrode materials (Schumacher et al., 2025). Economically feasible and industrially producible efficient electrocatalysts are needed as future energy fuels, such as hydrogen. Fuel cells that generate electricity from hydrogen need, in addition to proper electrocatalyst material, very stable and efficient electrolytes in terms of better ionic conduction and stability for a range of operating conditions (Wang et al., 2020). From the early 1900s, when Goldschmidt presented 'the method of chemical replacement,' which includes geometrical ion packing laws, ion radius ratios, and tabulated radii of cations and anions, the materials research community has been tackling this problem. Though crude, this model successfully predicted stable phases and structures. By 1926, most technologically important materials, still the objects of research today, were already known (though their properties remained unknown at the time: **semiconductor** and **piezoelectric** properties), including $BaTiO_3, AlN, ZnO\ and\ GaAs$ (Rost et al., 2015).

Research Question

How do different mixtures of Me^{2+} (Fe, Co, Mn, and Zn) cations in $Li_2[Me^{2+}]Cl_4$ affect the electronic Density of State (DOS)?

I. Single Me cation

II. Multi Me cation

Research Hypothesis

The enhancement and reduction of electronic conductivity depend on the increasing (decreasing) number of different mixtures of Me^{2+} cations in the $Li_2[Me^{2+}]Cl_4$, which can lead to changes in the electronic density of states.

Research Objective

The objective of this Master's thesis is the computation and analysis of the DOS of some selected Me^{2+} (Fe, Co, Mn, and Zn) cations in $Li_2[Me^{2+}]Cl_4$ compounds to identify electronic conductivity-related trends (Metals, Semiconductors, and Insulators) for a single-phase and multi-phase.

CHAPTER 1: LITERATURE REVIEW

CHAPTER 1: LITERATURE REVIEW

INTRODUCTION

The global transition toward renewable energy technologies has established the battery as a key player in modern energy storage devices, enabling mobility, portable electronics, and grid integration (Armand & Tarascon, 2008; Goodenough & Park, 2013). Lithium-ion batteries (LIBs), in particular, have become the standard due to their high energy density, long cycle life, and reliability (Tarascon & Armand, 2001). However, the effectiveness of conventional transition-metal oxide cathodes is limited by material scarcity, capacity loss, and economic barriers (Manthiram, 2020). In this context, high-entropy materials (HEMs) that exploit the concept of configurational entropy to stabilise multi-cation systems are gaining prominence as future electrode materials (Rost et al., 2015; Yeh et al., 2004). Subject to the moderate extent of the research so far conducted on high-entropy oxides with high stability and high-ionic conductivity (Sarkar et al., 2019), high-entropy chlorides (HECls) are relatively understudied. However, they offer tunable electronic as well as ionic characteristics that would aid battery performance (Zheng et al., 2023).

This chapter introduces the core principles underlying electrochemical storage, with an emphasis on the components of lithium-ion batteries, the constraints associated with traditional cathodes, and the recent advancements in high-entropy materials. Emphasis is placed on halide-based systems, especially chlorides, which signify a burgeoning area of research.

1.1 Batteries:

Batteries are a common type of electrochemical energy storage that can be found in everything (devices) ranging from power tools to medical equipment to personal electronics. They store charge through chemical reactions, usually by storing ions in a host material or converting a substance. They transport ions into a crystal framework through chemical reactions; this mainly leads to imperfect or limiting charging rates and low power densities. However, their reactions are not limited to a surface (unlike electrochemical capacitors), because of this, they (batteries) can achieve energy densities relative to capacitors (Price, 2023).

The needs and demand for more powerful electronic devices necessitate more suitable batteries; meanwhile, the development of batteries is progressing at a slower pace compared

to other areas in electronics, which results in issues like short lifetimes and lower capacities in modern batteries (Saxena et al., 2017; Starner, 2003). Additionally, we have seen a big investment in research on electric vehicles, with our objectives of leaving fossil-fuel-consuming vehicles behind us (Tollefson, 2008). The biggest challenge of moving from fossil fuels to electric vehicles is that of higher-capacity batteries; while current battery energies are around 200 Whkg^{-1} (Tian et al., 2021; Wang et al., 2018), we need at least 500 Wh$kg^{-1}$to meet the electrification of electric vehicles. This proposes an urgent need for higher capacity, robustness, and longer-life batteries (Price, 2023).

The 'intercalation' of lithium or other ions into layered materials is one method employed in newer batteries. Intercalation of ions into a host structure is a widely tested strategy for obtaining better electrochemical performance, including applications other than batteries, e.g., catalysts for water electrolysis. For example, there are different ion entry, diffusion, and exit mechanisms on discharge for some materials. Moreover, intercalation was employed to modify thermal (Holgate et al., 2013; Holgate et al., 2013), optical (Hanson et al., 2019; Hitz et al., 2016; Smith et al., 2020), and magnetic (Shkvarin et al., 2021) properties of materials. The newly reported metastable, superdense phases of lithium have been discovered to be formed when intercalation occurs in layered materials like graphite (Kühne et al., 2018; Zhou et al., 2022). The new phases of the material hold the promise of new properties and insight into the interaction of the materials with an intercalated species, and the development of the properties would be useful for different applications.

1.1.1 Battery Working Principle

All batteries have three fundamental elements: a positive electrode, a negative electrode, and an electrolyte. The battery operates by the movement of charged ions from the negative electrode to the positive electrode via the electrolyte by an electrochemical reaction. The reaction also produces electrons and thus electric energy to supply devices, as indicated in Figure 1.1. The process of charge transfer proceeds until the active materials are fully transformed. As a result, electrons no longer flow through the circuit, and the battery is unable to provide power (discharged state). By reversing all reactions, the battery needs to be charged to return to the starting point. Ionic and electronic forces within an operating battery always need to be balanced (Meena, 2021).

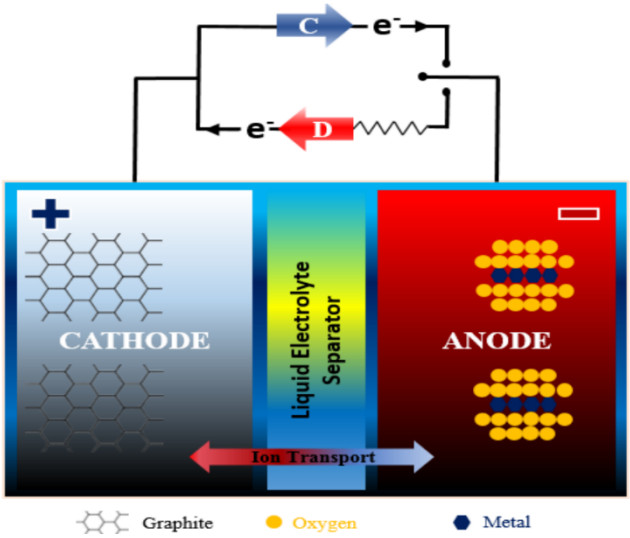

Figure 1.1: Schematic diagram of the battery working principle (Meena, 2021)

1.1.2 Components of Lithium-Ion Batteries (LIBs)

A lithium-ion battery (LIBs) is a rechargeable battery that uses lithium ions as a key material in its electrochemical reactions (Aida, 2022). When charged and discharged, the ions travel between the negative (anode) and positive (cathode) electrodes (Garche, 2024). Li-ion batteries have four constituents: the cathode, anode, electrolyte, and separator (Fig. 1.2). Each of these plays a significant role in the operation of the battery (Pender et al., 2020).

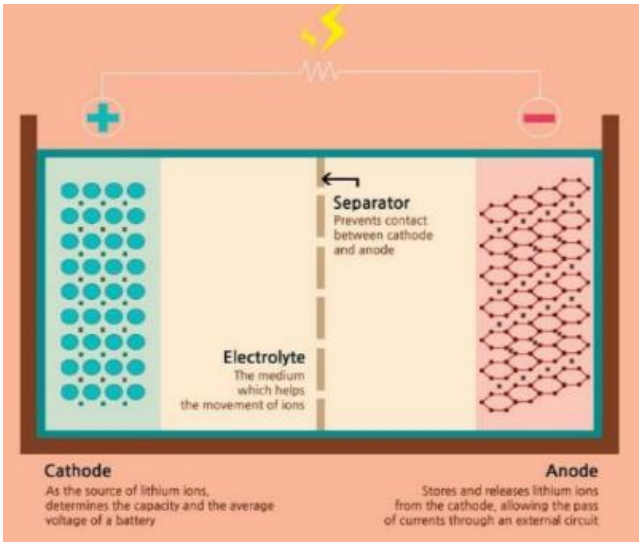

Figure 1.2: The lithium-ion battery's components (LIBs) (Aida, 2022).

- **Cathode**: The electrode where reduction takes place, i.e., the gain of an electron.
- **Anode**: The electrode where oxidation takes place, i.e., the loss of an electron

- **Electrolyte**: This is the central material between the two electrodes, namely anode and cathode, and it allows only the flow of ions and not the electrons, and they make the battery conductive.
- **Separator**: It prevents physical contact between the anode and cathode electrodes (Y. Wu, 2015).

The development of LIBs by John B. Goodenough, M. Stanley Whittingham and Akira Yoshino were a great advance over Ni-Cd batteries as they provided enhanced performance in terms of cycle life, safety, and rapid charging (Sato et al., 2020). LIBs are extensively utilised as a source of energy (Gong & Yang, 2011). Due to their high energy density, light weight, and versatility, they are used in products such as mobile phones, digital cameras, laptops, robots, and automobiles (Liu et al., 2019), with good capacity and cycling stabilisation (Wen et al., 2008). LIBs are also characterised by having long life cycles, soft self-discharge, and no memory effect (Ji et al., 2011). They provide the highest voltage, which is three times compared to other types of batteries like lead acid, nickel-metal hydride (Ni-MH), and nickel-cadmium (Ni-Cd). The batteries generate electricity through redox reactions (reduction and oxidation) between the two electrodes (Han et al., 2014). LIBs are also applied in improving kinetic performance and promoting catalysis by biomass pyrolysis or gasification (L. Chen et al., 2021).

1.1.3 Scheme of Lithium-Ion Batteries

Lithium-ion batteries are rechargeable batteries (Wei et al., 2020), and oxidation as well as reduction reactions occur when an electric charge is delivered and extracted (Bresser et al., 2016). Before a lithium battery can be used, it typically needs to be charged, and this moves electrons from the voltage source from the cathode towards the anode. Equilibrium is achieved when the lithium ions on the cathode shift into the electrolyte and separator and travel in the direction of the anode pole, indicating a charged battery (Zhu et al., 2018).

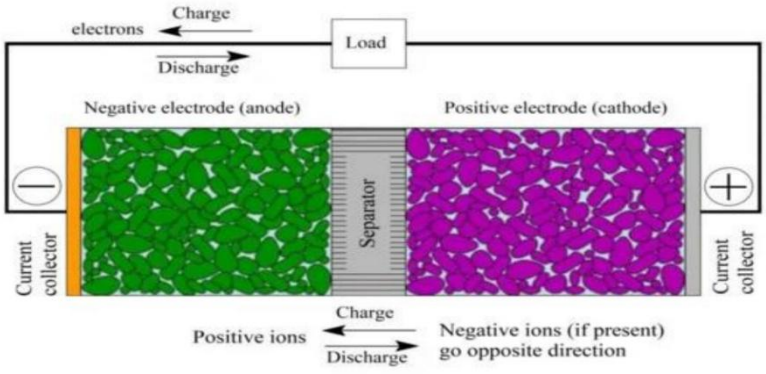

Figure. 1.3: The detailed scheme of a lithium-ion battery (Al-Gabalawy et al., 2020).

The reverse is the case when lithium batteries are utilised. Electrically charged electrons proceed from the anode pole to the cathode pole through the load. During this process, lithium ions move from the anode pole to the cathode pole through the electrolyte and into the pores of the separator, as seen in Figure 1.3 (Al-Gabalawy et al., 2020). The anode reaction is the process through which the anode supplies electrons to the external circuit during discharge. During charging, the cathode reaction accepts electrons from the external circuit. Figures 1.4 and 1.5 illustrate the electrochemical response when charging and discharging for clarity.

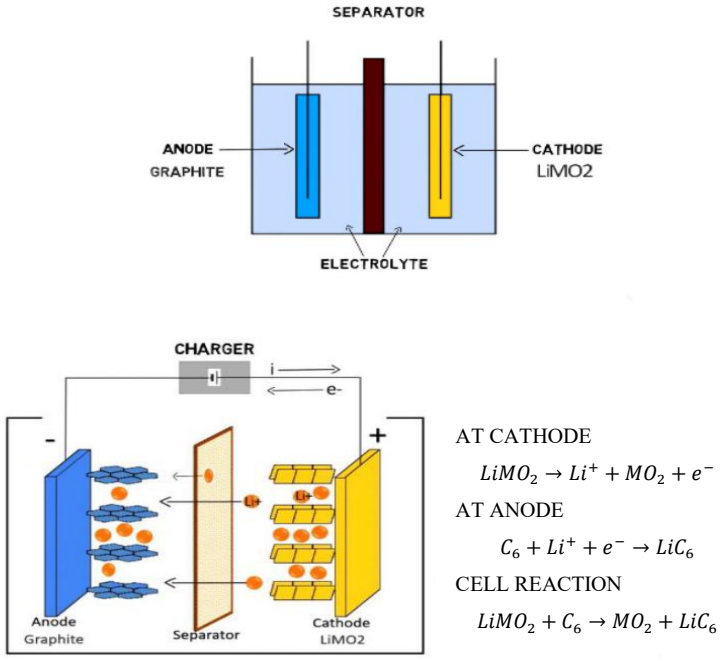

Figure 1.4: Electrochemical reactions that occur during charging.

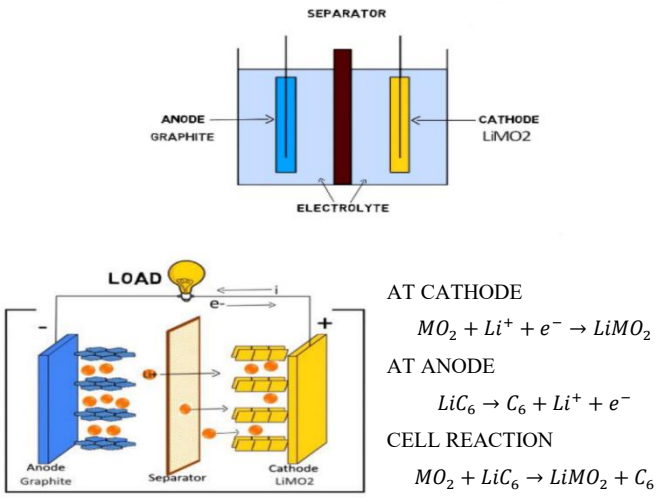

Figure 1.5: Electrochemical reactions during discharge.

The overall reaction can be summarised as follows:

Positive electrode (M: transition metal):

$$\text{Charge: } LiMO_2 \rightleftharpoons Li_{1-x}MO_2 + xLi^+ + xe^-$$

$$\text{Discharge: } Li_{1-x}MO_2 + xLi^+ + xe^- \rightleftharpoons LiMO_2$$

Negative electrode:

$$\text{Charge: } C + xLi^+ + xe^- \rightleftharpoons Li_xC$$

$$\text{Discharge: } Li_xC \rightleftharpoons C + xLi^+ + xe^-$$

Overall reaction:

$$\text{Charge: } LiMO_2 + C \rightleftharpoons Li_xC + Li_{1-x}MO_2$$

$$\text{Discharge: } Li_xC + Li_{1-x}MO_2 \rightleftharpoons LiMO_2 + C$$

Discharge lithium-ion:

$$\text{Anode (-): } LiC_6 \rightarrow C_6 + Li^+ + e^-$$

$$\text{Cathode (+): } MO_2 + Li^+ + e^- \rightarrow LiMO_2$$

$$\text{Overall: } LiC_6 + MO_2 \rightarrow C_6 + LiMO_2$$

1.1.4 Function of Batteries

A typical Li-ion cell (Figure 1.6) highlights the two main components: the electrodes and the electrolyte. Other components, such as the 'separator' (which physically separates electrodes to prevent shorting), the 'current collector' (which connects components that collect electrical current to external circuits), and the 'binder' (which binds active materials in the electrodes), may be included during manufacturing. These additional components do not participate in electrochemical processes but instead increase the cell's efficiency, lifetime, and performance (Price, 2023).

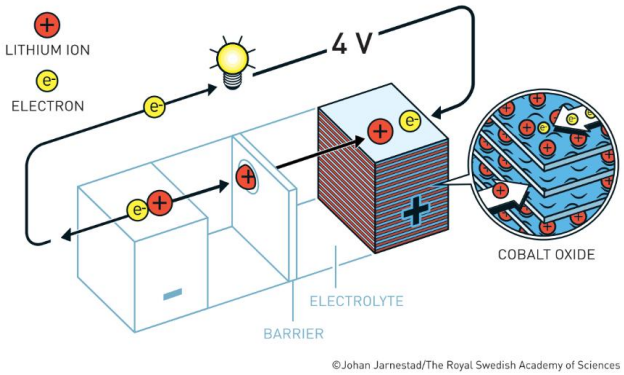

Figure 1.6: Schematic of Goodenough's battery during discharge, with a $LiaCoO_2$ cathode. Figure reproduced from the Nobel Prize Website (Wu, 2015).

1.1.5 ELECTRODES

The electrodes of electrochemical cells are where electrochemical reactions happen. Such reactions in an intercalation battery involve intercalation and deintercalation of ions. The electrodes are tasked with 'accommodating' the intercalated ions when charging and discharging. Although theoretically there is no limit to what these intercalated ions would be, lithium will be used as an example in the following discussions.

The direction of ions and electrons reverses at the time of charging by reversing this allotment of duties; however, in accordance with consistency, only discharge operations will be explained within this master's thesis.

For intercalation electrodes, Whittingham initially suggested that layered-structure materials with van der Waals spacings would be suitable for storage of intercalant species (Whittingham, 1976). The spacings are natural pores for lithium and facilitate reversible intercalation reactions without bond breaking. For the standard lithium-ion battery with a graphitic anode and $LiCoO_2$ cathode, the discharge reaction can be expressed as:

$$\text{Cathode: } CoO_2 + aLi^+ + ae^- \rightarrow Li_aCoO_2$$

$$\text{Anode: } Li_aC_6 \rightarrow C_6 + aLi^+ + ae^-$$

$$\text{Full Reaction: } Li_aC_6 + CoO_2 \rightarrow C_6Li_aCoO_2$$

Such a reaction, or an equivalent reaction involving other electrode materials, generates a potential difference between the cells. The potential difference is a significant parameter in electrochemistry, to which the various electrode materials can be described and compared. To enable easy comparison of intercalation potentials of various materials, the reference anode made of lithium metal is generally used. This provides the electrode half-cell potential for any given material, i.e., the voltage relative to the Li/Li^+ redox potential (Bard & Faulkner, 2001).

These ideal cathode materials exhibit high voltage compared to the Li/Li^+ redox level, with present market leaders reaching 3-5 V (Andersson et al., 2000; Li et al., 2009; Liao et al., 2012; Y. Liu et al., 2013; Lung-Hao Hu et al., 2013; Lyu et al., 2021; R.N. et al., 2020). Ideal anodes, on the other hand, exhibit a low (but positive) voltage. The voltage between any two paired materials may be known from their difference. For example, $LiCoO_2$ is $\sim 4\ V$ (Lyu et al., 2021), and graphitic carbon receives voltages as low as 0.01 V (Asenbauer

et al., 2020), which allows cells that use these materials to be able to supply a 4 V battery.

1.1.6 Conventional Batteries

Very few materials are intrinsically suitable for battery use and therefore must be meticulously chosen according to their intrinsic properties. Conventional lithium-ion liquid electrolyte batteries dominate the market, ranging from portable electronics to high-energy uses like electric vehicles. Nevertheless, because of the flammable liquid electrolyte, they still suffer from safety concerns and costly packaging, thus calling for development. Nanotechnology, new materials, and replacing or stabilising solid electrolytes with liquid electrolytes are hence employed to improve Li-ion batteries(Meena, 2021).

1.2 High-Entropy Materials (HEMs)

High-Entropy Materials (HEMs) are defined by four key properties: high configurational entropy, severe crystal lattice distortion, diffusion effects, and cocktail or composite effects (Gao et al., 2016). HEMs are made of a solitary crystal lattice where different elements, often transition metals, occupy the same locations on the crystal lattice (Cantor et al., 2004; Yeh et al., 2004). These multi-component systems are distinguished by their structural complexity and demonstrate increased cycle stability, exceeding the performance of standard oxide materials (Schumacher et al., 2025). These phases can be regarded as very complicated solid solutions (Cantor et al., 2004; Yeh et al., 2004). These effects, functioning in concert, support the thermodynamic stability, kinetic behaviour, and functional performance of HEMs, typically enabling fewer phases than expected by the Gibbs phase rule (Miracle & Senkov, 2017; Murty et al., 2014).

The possible use of high-entropy materials in batteries has lately attracted substantial interest. Compared to typical materials, high-entropy materials demonstrate high defect density and internal entropy, leading to increased ion storage capacities, ionic conductivity, and electrochemical stability.

The high-entropy approach has now been expanded to additional chemical systems and disciplines, including the production of materials for electrochemical applications (Yan et al., 2020). HEOs and fluorides have been reported to be synthesised in rocksalt (Lun et al., 2021), fluorite (Ying et al., 2021), perovskite (Jiang et al., 2018), and spinel structure types (Mao et al., 2020). Depending on cation size, oxidation states, and synthetic factors, a range of HEM phases may be formed within these conventional structural types (Gao et al., 2016; Szymanski et al., 2023; Q. Wang et al., n.d.; R. Z. Zhang & Reece, 2019). These structural

types display strong lattice distortion and diffusion effects, arising from cation or anion size mismatches, preferred coordination, and spin states within a multi-component system. This can lead to variations in bond lengths, unit cell size, or symmetry. The influence of considerable lattice distortion is found in material characteristics as magnetism, electrochemical activity, electrochemical stability, and catalytic activity (Mao et al., 2020; Wang et al., 2020; Yao et al., 2022). Additionally, crystallographically different locations inhabited by various elements can be partly replaced by alkali metal cations, improving ion mobility. This behaviour has been reported in perovskite (Itoh et al., 1994) and garnet structures (Kokal et al., 2011; Kumar et al., 2016). Finally, cocktail or composite effects explain synergistic effects from combining certain cations in molar ratios inside a single crystal lattice, leading to increased material properties (Gao et al., 2016).

1.3 FOUR KEY PROPERTIES (EFFECTS) OF HIGH-ENTROPY MATERIALS

1.3.1 High-Entropy Effect

The defining feature of HEMs is their enhanced configurational entropy (S_{config}), which derives from the random distribution of numerous main elements over equivalent lattice sites. For an *N*-component solid solution, S_{config} is provided by:

$$S_{config} = -R[(\sum_{i=1}^{N} x_i lnx_i)_{cation-site} + (\sum_{j=1}^{M} x_j lnx_j)_{anion-site}]$$

where x is the mole fraction of each element, N and M are the number of species that can occupy each site, and R is the gas constant. This entropy contributes to the entropy of mixing (ΔS_{mix}), which occurs in the Gibbs free energy of mixing:

$\Delta G_{mix} = \Delta H_{mix} - T\Delta S_{mix}$ (2.3)

For a binary regular solution:

$\Delta H_{mix} = \beta X_A X_B$ (2.4)

where β depends on the interaction between components. Since ΔS_{mix} is always positive, the term $-T\Delta S_{mix}$ is negative, encouraging phase stability. In HEMs, sufficiently large $-T\Delta S_{mix}$ can overcome positive enthalpy penalties, stabilising single-phase solid solutions at high temperatures. However, many such phases are metastable at ambient temperature, and ΔH_{mix} and T still play key roles in defining phase composition (Miracle & Senkov, 2017; Murty et al., 2014)

1.3.2 Sluggish Diffusion Effect

Diffusion in HEMs is expected to be slower than in conventional alloys (Tsai et al., 2013; Tsai & Yeh, 2014), in large part due to local chemical complexity. The variations in atomic environments create a distribution of bonding energies, developing low-energy sites that trap atoms and high-energy sites that repel migration. The heterogeneous energy landscape can suppress atomic mobility, retarding phase segregation and allowing metastable phase retention. While there are some studies questioning the universality of such an effect (Divinski et al., 2018), slow diffusion is typically connected with such properties as improved creep resistance (Lee et al., 2017).

1.3.3 Lattice Distortion Effect

Even with the selection of elements of similar atomic radii, considerable size mismatches are likely in HEMs having five or more elements. These mismatches disrupt the crystal lattice, influencing structure-sensitive characteristics. Lattice distortion can hinder dislocation motion, resulting to substantial solid-solution strengthening, as observed in many high-entropy alloys (HEAs) (Senkov et al., 2011).

1.3.4 Cocktail Effect

The cocktail effect is the synergy of a number of principal components to form properties not predictable by the rule of mixtures (Ranganathan, 2003). Such synergies may arise from interactions between components that are intricate and form unforeseen structural or property changes. An example is the addition of Al to an fcc Co–Cr–Cu–Fe–Ni alloy—expected to soften it, actually forming a bcc structure and hardening (M. H. Tsai & Yeh, 2014).

1.4 Interconnection of the Primary Effects

Thermodynamically, the high-entropy effect stabilises phases, and sluggish diffusion kinetically stabilises metastable states at low temperature. Mechanical and functional properties are largely dominated by lattice distortion and the cocktail effect. The coexistence of all four effects makes HEMs a unique category of materials with unprecedented stability, strength, and functionality combinations.

1.5 HIGH-ENTROPY ALLOYS (HEAS)

The notion of HEAs was originally developed in 2004, combining various metals to generate new components with five or more elements (Cantor et al., 2004; Yeh et al., 2004). HEAs have been employed to offer a balance of characteristics in multicomponent alloy systems (Yeh et al., 2004). Since then, the high-entropy idea has been extensively applied in metallurgy, where such HEAs exhibit extraordinary resistance against corrosion and enhanced wear resistance (Zhang et al., 2014). HEAs offer strength-ductility synergy (Ma & Wu, 2019), produce outstanding electrocatalysts (Löffler et al., 2021) and supercapacitors (Hussain et al., 2021; Xu et al., 2020), and are utilised in rechargeable batteries (Chen et al., 2021). Numerous high-entropy chemicals have been effectively employed in various complex materials examined by HEAs (Musicó et al., 2020).

1.6 HIGH-ENTROPY OXIDES (HEOS)

The high-entropy notion was applied to oxides for ceramic applications starting in 2015 (Rost et al., 2015). High-entropy oxides (HEOs) are defined as oxides having five or more components in a single-phase oxide system and configurational entropy (S_{config}) larger than 1.5R (where R is the universal gas constant) (Sarkar et al., 2020). (Rost et al., 2015) first accomplished HEO with effective stabilisation entropy in 2015, employing equimolar amounts of five oxides (MgO, NiO, CuO, CoO, and ZnO) in a rock salt framework. It was established that configurational entropy is maximised with an equimolar stoichiometry, which promotes the creation of single-phase HEOs (Rost et al., 2015).

HEOs have been intensively researched as possible materials for electrode and electrolyte applications (Sarkar et al., 2018). HEOs display strong Li-ion conductivity (10^{-3} S cm^{-1}), which is more than two orders of magnitude greater than LiPON (lithium phosphorous oxy-nitride) solid electrolyte (Bérardan et al., 2016). This makes them promising for numerous possible applications.

HEOs are particularly explored for their possible usage as cathode or electrolyte materials in batteries (Schumacher et al., 2025). HEOs were originally reported as anode materials for LIBs by Sarkar in 2018 (Sarkar et al., 2018). High configurational entropy can give major advantages for storage capacity retention and greatly increase cycling stability (Sarkar et al., 2018). The increased defect density in HEOs also boosts ionic conductivity, resulting in reduced activation energies (Sarkar et al., 2018). The defect hopping process (shown in Figure 1.7 High-entropy nitride and 1.8) (Van Der Ven et al., 2013) is greatly

improved owing to the migration of Li cations into transition metal sites inside a crystal structure (Zeng et al., 2022). High-entropy effect on a spinel-type structure: Extreme lattice distortion from size mismatches results in broader migration paths, partial substitution of Li and (partial) vacancy on tetrahedral sites results in weaker Li on octahedral sites, which causes enhanced probability for divacancy and Li-Li interaction, greater possibility of vacancies and partial substitution with triple vacancy hops (Schumacher et al., 2025).

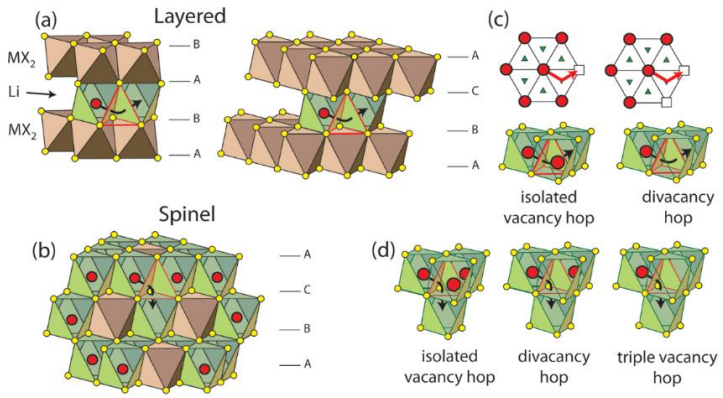

Figure 1.7: Ionic diffusion mechanisms via Li-Ion hopping in layered (a, c) and spinel structures (b, d) as modelled by Van Der Ven et al. (Van Der Ven et al., 2013).

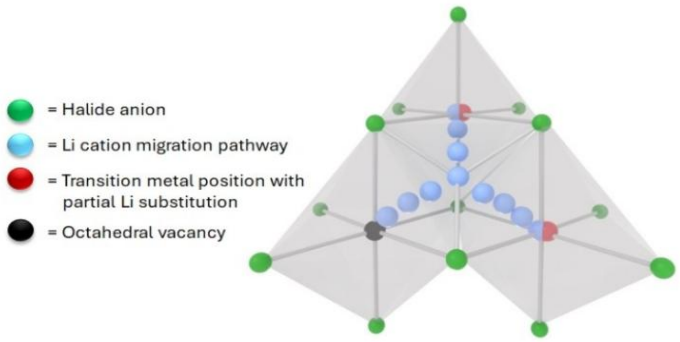

Figure 1.8: High-entropy effect on a spinel-type structure(Schumacher et al., 2025).

In conventional systems, ion transport occurs on sites with equal energy levels when site energy distributions overlap. However, adding cation disorder in a HEM disturbs high-energy sites, decreasing the energy barrier between Li-occupied sites while enhancing it in low-energy sites. This produces a percolating network of "similar-energy-nearest-neighbour-sites" (Zeng et al., 2022) which boosts ionic conductivity and diffusion processes in HEMs. The energy needed for an isolated vacancy hop in spinel and hexagonal/trigonal layered structures relies on the occupancy of tetrahedral sites and the resulting lattice distortion. Partial substitution on both tetrahedral and octahedral sites,

which would ordinarily be filled by transition metals or lithium in conventional materials, results in lower Li-Li interactions, favouring solitary vacancy hops. Introducing lanthanides like Tb can generate a significant degree of lattice deformation and partial vacancy of tetrahedral sites in spinel structures. Lanthanides also prevent the production of a tetragonal phase during cycling and stabilise the cubic spinel phase, boosting cycling stability and rate capability (Hou et al., 2023). The enhancement of the diffusion mechanism in spinel-type high-entropy materials is attributed to high configurational entropy, leading to lithium displacement onto transition metal positions, lessened Li-Li interaction, and broader migration pathways due to severe lattice distortion, all contributing to an increased likelihood of Li^+ diffusion processes.

Subsequently, the high-entropy idea was applied to oxyhalide (Wang et al., 2021) and fluoride perovskites (Wang et al., 2020) electrode materials in batteries (Wang et al., 2021). A high-entropy oxide perovskite with the composition $[((\mathrm{Bi,Na})_{0.2}\ (\mathrm{La,Li})_{0.2}\ (\mathrm{Ce,K})_{0.2} Ca_{0.2}\ Sr_{0.2}]\ TiO_3$ was employed as an anode material for lithium-ion batteries (Yan et al., 2020). High-entropy rocksalt oxyfluorides, such as $\mathrm{Li}_{1.3}\mathrm{Mn}_{0.2}\ \mathrm{Mn}_{0.2}\ Ti_{0.1}\mathrm{Nb}_{0.2}\ \mathrm{O}_{1.7}\mathrm{F}_{0.3}$ (Lun et al., 2021), are employed as cation-disordered rocksalt cathodes where Li^+flows via a percolating network of 0-TM (transition metal) clusters.

1.7 HIGH-ENTROPY CHLORIDES (HECLS)

High-entropy chlorides (HECls) are part of a family called high-entropy materials (HEMs) and specifically high-entropy halides (HEHs).

High-entropy chlorides can be synthesised by a liquid synthesis method, examples are high-entropy chlorides perovskites like $K[MgMnCoNiZn]Cl_3$ and $K[MgMnFeCoNiZn]Cl_3$ (Wang et al., 2020). The result of this, when compared to the market value of IrO_2 showed increased electrocatalytic activity. While high entropy chlorides show good cycling stability, due to their entropy stabilisation effect, lattice distortion, and specific capacity, there are still no applications of high entropy chlorides in battery applications. Li_2FeCl_4 (Payne et al., 2018) and Li_2MnCl_4 are shown as a promising material due to their strong cycle stability against lithium and cheap manufacturing costs (Liu et al., 2024; Schumacher et al., 2025). These materials show potential as cathode materials and can be crystallised in $Fd\bar{3}m$ cubic anti-spinel structure and is known as the basis for high-entropy halide spinel-type structure materials; furthermore, halide spinel structures such as Li_2FeCl_4 has shown

good ionic conductivities (Kanno et al., 1981). They not only have low production cost but also good cycling stability against lithium. High-entropy oxides and an extent of some high-entropy halides have been shown as promising materials for sodium-ion batteries (SIBs) as potential electrode materials. High-entropy materials have a broad selection of possible stoichiometries and compositions, and this opens a broad investigation and the tailoring of various desirable properties for application in any field currently (S. Yan et al., 2022).

CONCLUSION

In short, Chapter 1 outlined the fundamental theory and technology required in understanding the issues of the present LIBs and proposed high-entropy materials as an alternative. High-entropy chlorides were determined as an unstudied yet promising series of compounds, and hence the reason behind the current exploration using computational approaches. Upon this foundation, Chapter 2 sets out the computational framework and software used in the current exploration.

CHAPTER 2: MATERIAL AND METHODS

CHAPTER 2: MATERIAL AND METHODS

INTRODUCTION

Computational simulation is an invaluable aid in the exploration of high-order functional materials, specifically in the scenario when experimental synthesis is elaborate and costly (Hafner, 2008; Martin, 2004). The density functional theory (DFT), founded on the Hohenberg–Kohn theorems and the Kohn–Sham formulation, is an efficacious quantum-mechanical approach used in the prediction of the structure as well as electronic characteristics (Hohenberg & Kohn, 1964; Kohn & Sham, 1965).

This chapter explains the theoretical and computational methodologies applied in this work. It begins with a brief introduction of quantum mechanics pertinent to electronic structure, before introducing density functional theory and its limits. The use of DFT+*U* is then presented in the context of transition-metal chlorides. Lastly, the practical aspects of the computational protocol are discussed, including the use of the Quantum ESPRESSO code for structure relaxations, density of states calculations, and parameter fitting.

2.1 AB INITIO DENSITY FUNCTIONAL THEORY

The terms "*ab initio*" and "first principles" have been widely used in various fields of science, such as physics, materials science, mechanical engineering, electronics, chemistry, biology, and so on. The core notion of these terms is to regard the many-atom systems as many-body systems, which are composed of electrons and nuclei, and to treat everything without introducing any empirical parameters based on the first principles of quantum mechanics (Ohno et al., 2003).

First-principles (or *ab initio*) helps in the study of the electronic structures of solids, surfaces, or clusters as accurately as possible with moderate computational effort. Additionally, the usage of *ab initio* molecular-dynamics methods helps us in calculating the forces exerted on atoms at each time step, and one can do the simulation of the evolution of atomic and electronic motions without the assumption of empirical parameters. The mass of an electron is very small compared to the mass of the nuclei; hence, electrons move very quickly so as to follow the nuclear motion. In the above case, where the electronic state occurs very rapidly compared to the nuclear motion, the assumption that is been made that the electrons are always in a steady state generally holds, and this is called the Born-Oppenheimer adiabatic approximation. This approximation method sets the basis of the usual *ab initio* molecular-dynamics methods, and the usage of this approximation we can

separate the calculation of the electronic structure from that of the ionic motion and perform the two calculations separately in each step (Ohno et al., 2003).

Nevertheless, the quantum states of many-electron systems are not as easy as they seem, even with the most sophisticated methods of modern physics and chemistry; therefore, one must rely on some approximating theories, and these methods are reliable but not exact (Ohno et al., 2003).

Approaching the many-atom systems for the ground states and excited states, there are many first-principles approaches, and these approaches are classified into four main groups, namely: Density Functional Theory, Hartree-Fock approximation, Green's Function approach, and the Monte Carlo methods. The first approach will be discussed in this work.

2.2 SCHRÖDINGER'S TIME-INDEPENDENT EQUATION

The time-independent Schrödinger equation is one of the main goals in quantum chemical approaches for approximating electronic structure.

It is given by:

$$\hat{H}\psi_i = E\psi_i$$

Where $\hat{H}$ is the Hamiltonian operator which consists of M nuclei and N electrons in the absence of magnetic or electric fields, ψ_i is the molecular wave function, and E is the molecular total energy. $\hat{H}$ is a differential operator that represents the total energy:

$$\hat{H} = \hat{T} + \hat{V} = \hat{T}_N + \hat{T}_e + \hat{V}_{NN} + \hat{V}_{ee}$$

Also, where $\hat{T}$ is the kinetic energy of the particles, $\hat{V}$ is the potential energy of the particle pairs. Hence, we can write Schrödinger's time-independent equation with the Hamiltonian (where the electron mass is denoted by m here, kinetic energy of each electron, the interaction energy between each electron and the group of atomic nuclei, and the interaction energy between various electrons are defined, in order, by the three terms in brackets in this equation:

$$\left[\frac{h^2}{2m}\sum_{i\ 1}^{N}\nabla_i^2 + \sum_{i\ 1}^{N}V(r_i) + \sum_{i\ 1}^{N}\sum_{j<i}U(r_i, r_j)\right]\psi = E\psi$$

2.3 DENSITY FUNCTIONAL THEORY

The general notions of the DFT of quantum systems were initially suggested by Thomas and Fermi in 1927 (Barghamadi et al., 2013; Huang et al., 2022).

From the original Thomas-Fermi technique, the potential energy at any given position is equal to the electron density and the local density at that position. In contrast, the kinetic

energy of the electrons is approximated as an explicit function of the density. Although this approximation is basic, it then lacks the essential chemistry and physics of an N-electron system. In 1964, Hohenberg and Kohn (Hohenberg & Kohn, 1964) put up two crucial theorems that allowed DFT to reach extraordinary development.

Theorem I: The external potential (and consequently the total energy) is a unique functional of the electron density.

$$\boldsymbol{E = E[n(\vec{r})]}$$

Theorem II: The function that provides the ground-state energy of the system gives the lowest energy if and only if the input density is the actual ground-state density.

$$\boldsymbol{E[n(\vec{r})] > E_o[n_o(\vec{r})]}$$

Thus, the Hohenberg-Kohn theorem demonstrated the existence of a general density functional that linked the energy of a system to its electron density distribution but did not propose a method for building this functional. This boils down to the Kohn-Sham approach, (Kohn & Sham, 1965; Peng et al., 2016) where the design of an auxiliary system hinges upon two assumptions: (1) The exact ground state density can be represented by the ground state density of an auxiliary system of non-interacting particles. (2) The auxiliary Hamiltonian is calculated to have the normal kinetic operator and an effective local potential $V_{\sigma eff}(r)$ acting on an electron of spin σ at point r.

The Kohn-Sham approach to the full interacting many-body issue is to recast the Hohenberg-Kohn expression for the ground state energy functional in the form:

$$\boldsymbol{E_{KS} = T_S[n] + \int drV_{ext}(r)n(r) + F_{Hartree}[n] + E_{II} + E_{xc}[n]}$$

Here, $\boldsymbol{V_{ext}(r)}$ denotes the external potential which is caused by the nucleus and any other external fields. E_{II} is the interaction between the nuclei. Ts is the independent-particle kinetic energy, which is given by:

$$\boldsymbol{T_S = -\frac{1}{2}\sum_{\sigma}\sum_{i=1}^{N^\sigma} < \psi_I^\sigma|\nabla^2|\psi_I^\sigma > = \frac{1}{2}\sum_{\sigma}\sum_{i=1}^{N^\sigma}\int d^3r|< \nabla\psi_I^\sigma >|^2}$$

and the classical Coulomb interaction energy of the electron density n(r) interacting is defined as:

$$\boldsymbol{E_{Hartree}[n] = \frac{1}{2}\int d^3r\, d^3\acute{r}\,\frac{n(r)n(\acute{r})}{|r-\acute{r}|}}$$

Besides, all the many-body effects involving exchange and correlation are bundled into the exchange-correlation energy $\boldsymbol{E_{xc}}$ that can be represented as:

$$\boldsymbol{E_{xc}[n]} = < \widehat{\boldsymbol{T}} > - \boldsymbol{T_S[n]} + < \widehat{\boldsymbol{V}}_{\boldsymbol{int}} > - \boldsymbol{E_{Hartree}[n]}$$

Here, [n] signifies a functional of the density n (r, σ) which depends upon both position in space r and spin σ. Through the Kohn-Sham approximation, a complicated multi-electron problem can be converted into a single-electron problem.

In general, with the development of DFT theory, practically all the materials can be explained and predicted well by DFT theory, and the computational efficiency has been substantially increased.

2.4 X Exchange-Correlation Functional in Density Functional Theory

The exchange-correlation (XC) functional is the key approximation in density functional theory (DFT), and the accuracy greatly determines the method's power in describing properties of real materials. It is theorised in the Hohenberg–Kohn theorems (Hohenberg & Kohn, 1964) that any ground-state properties of a system with interacting electrons can only be solely described through the electron density. The Kohn–Sham formulation transforms the many-electron problem in such a system back into a set of single-particle equations in conjunction with an effective potential, where the exchange-correlation part, $E_{xc}[\rho]$, takes in all the unidentified quantum many-electron phenomena, including electron exchange and correlation (Kohn & Sham, 1965). Because there does not exist a closed real analytical form for E_{xc}, realistic applications of DFT require utilising approximate functionals, and the current challenge in trying to improve such approximations remains central in the areas of theoretical chemistry and condensed matter physics.

2.4.1 Local and Semilocal Approximations

The first approximation to widely gain acceptance is the Local Density Approximation (LDA), where the exchange-correlation energy at a particular point in space is approximated solely on the basis of the local electron density, using the model of a uniform electron gas (Parr & Yang, 1989). While LDA adequately describes simple metals and smooth-density-gradient systems, LDA systemically overbinds molecules and solids, underestimates band gaps, and poorly handles inhomogeneous systems (Perdew & Zunger, 1981). Because of the aforementioned (LDA), the electron density and the gradient of the electron density as parameters was introduced in the General Gradient Approximation

(GGA). Perdew–Burke–Ernzerhof (PBE) type functionals improved bond length evaluation, atomization energy, and surface properties (Perdew, Burke, et al., 1996). However, GGAs continue to suffer from self-interaction errors and tend to underestimate van der Waals forces and band gaps as well (Cohen et al., 2008). In this master's thesis we used PBEsol exchange-correlation functional, which is a slight modification of PBE functional that allows for more accurate description of the ionic structure (Perdew et al., 2008).

Yet another breakthrough was attained through the definition of the meta-GGA functionals, with kinetic energy density as a further ingredient. Prominent success was the Tao–Perdew–Staroverov–Scuseria (TPSS) meta-GGA, conceived to fulfill rigorous constraints without empirical fitting and achieving superior performance for both molecules and solid-state materials (Tao et al., 2003). More recently, the SCAN (Strongly Constrained and Appropriately Normed) was introduced as a nonempirical functional fulfilling all 17 known exact constraints and thereby achieving a balanced level of accuracy for a vast set of systems (Sun et al., 2015). Such advances represent successive steps along "Jacob's Ladder" of DFT approximations, a phrase coined by Perdew to represent the evolutionary trajectory from LDA towards the "heaven" of chemical accuracy (Perdew & Schmidt, 2001).

2.4.2 Beyond-Semilocal and Hybrid Function

Despite the success of semilocal functionals in a wide array of systems, they remain inadequate in situations where electron localisation and strong correlation are important. To overcome these difficulties of electron localisation correlation, we implemented the exact Hartree-Fock exchange into the GGA scheme, thus reducing the deficiencies in self-interaction; hence, the Hybrid functionals. Examples range from B3LYP to HSE06, having seen widespread use in quantum chemistry and solid-state physics, respectively (Becke, 1993b; Heyd et al., 2003). Nonetheless, in spite of their success, hybrid functionals remain computationally intensive for larger scales and are at times poor in transferability for different chemical environments.

More recent projects have since tried to marry hybridisation with systematic constraint satisfaction methods. An example of the classic kind is the coupling of corrected density functionals and the Random Phase Approximation (RPA), to make better energy predictions at reduced computational cost than exhaustive post-DFT schemes (Graf & Thom, 2023). Parallel benchmarking initiatives highlight a common problem: no functional

offers uniformly high accuracy in the very wide range of chemical and material tasks without exception, and thus the necessity for ongoing refinement (Peverati & Truhlar, 2014).

For applications related to energy storage, for example, for high-entropy chlorides presented in the present master's thesis, it is not a minor consideration but a crucial deciding aspect to choose an exchange-correlation (XC) functional. Prediction sensitivity regarding band gaps, magnetic properties, and charge localised phenomena depends significantly on exchange and correlation treatment. Notably, for transition metal-containing systems, a significant correlation effect is present, and thus corrections in the form of DFT+U or higher-functionals are requisite in order to attain reasonable output (Anisimov et al., 1991). Hence, knowing the evolution and performance of XC functionals is essential for the correct conclusion of computational studies involving electrode materials.

2.5 ELECTRONIC PROPERTY

Electrical conductivity, another need for battery materials, may be assessed using the electronic structure. Energy band structures, density of states (DOSs), and charge density distribution are among the electronic characteristics of electrode materials that are frequently studied in order to assess their performance (Fan, 2022).

2.6 BAND STRUCTURE

The electronic band structure specifies the range of energy levels that the electrons within a specific material may have, and it is closely related to the conductivity (Danuta & Juliusz, 1962). The band structure of a solid material may be broadly classified into three well-established parts: the conduction band, the valence band, and the forbidden energy band gap (specifically in semiconductors and in insulators). For an insulator material, the band gap between the conduction and the valence band is relatively broad, making it highly unlikely for electrons to move or jump from the valence band to the conduction band. In other words, insulators are incapable of electricity conduction. For semiconductors, on the other hand, the band gap is very narrow (usually in the range of 0.5 to 3 eV). The electrons in the valence band are able to transition to the conduction band (e.g., as a result of temperature increases), hence forming conductive carriers. For the metallic band structure, the conduction band and the valence band overlap each other so that electrons are able to move to the conduction band freely and hence support high conductivity. It is important to note that semiconductors may be further subdivided into direct band gap and indirect band

gap semiconductors depending on the difference in paths electrons move through from the valence band to the conduction band within the first Brillouin zone (A. Kumar & Ahluwalia, 2012; Yuan et al., 2018).

2.7 Density of States

Density of states (DOS) determines the number of states present at a given energy level and available to be occupied by electrons; it is simply a measure of the number of electron states per unit energy and volume (He et al., 2019). Basically, the DOS is a more understandable form of the band structure. From DOS analysis alone, it is possible to examine the energy gap features as well. A zero DOS at the Fermi level implies the system might be an insulator or semiconductor; otherwise, a non-zero DOS is an indication of a metallic character in the system. The partial density of states (PDOS), relating to individual atoms or orbitals, may provide additional sophisticated bonding information. The recent study on DOS by Xiao and co-workers showed evidence proving how the incorporation of Li^+ into penta-graphene is capable of transforming its electronic structure and enhancing the electrochemical performance of lithium-ion batteries (LIBs) (Xiao et al., 2016). The pure penta-graphene itself is a semiconductor material with an expected band gap of 2.33 eV. With the addition of one lithium atom into the penta-graphene (LiC54), this hybrid system turned metallic (Fig. 2.1). As the ratio of lithium is increased (LiC3 and LiC1.5), the electronic conduction in penta-graphene is enhanced even further. This semiconductor-to-metal transition reduces the charging and LIBs' discharging rates considerably.

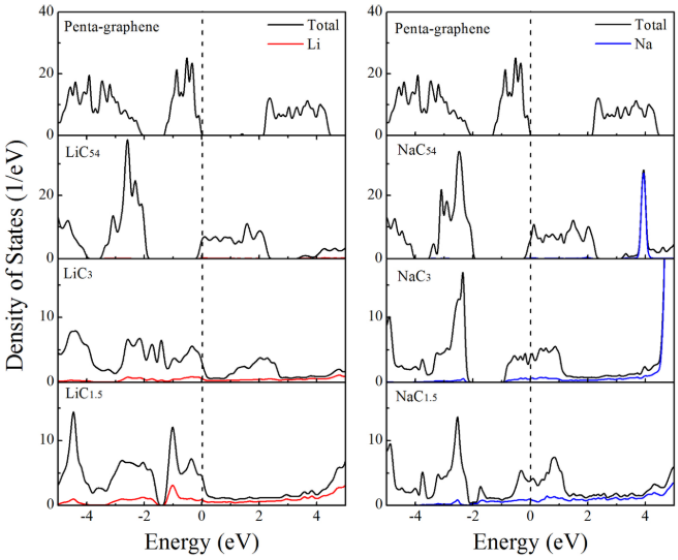

Figure: 2. DOSs of penta-graphene, LiC54, LiC3, and LiC1.5. (Xiao et al., 2016).

The acquisition of a precise description of electronic structure is crucial for predicting further electronic-related features, including intermolecular interactions and formation energies. The Hubbard model will therefore offer a straightforward technique to appropriately characterise the behaviour of materials with highly correlated d and /or f electrons, known as the Mott insulators. Based on the Hubbard model, the DFT+U methodology is designed, which is computationally convenient for accurate computations of electronic structures (Tolba et al., 2018).

DFT is one of the easiest and most used calculable methods of computation to anticipate and predicting the many properties of materials (Koch & Holthausen, 2001; Mattsson et al., 2005). While its accuracy is very good as regards structural and cohesive properties, it falls considerably behind in anticipating electrical and other related properties of semiconductors by as much as a factor of two (Seidl et al., 1996). Nevertheless, the accurate description of electronic structure is the foundation for prediction of other electronic-related properties, such as intermolecular interaction and formation energies. For the resolution of this problem, higher level computationally intensive calculations have to be used, utilizing more expensive computational schemes like hybrid functionals, which require the solution of the exact Hartree-Fock (HF) equations, as a quest to achieve substantially higher accuracy (Sholl & Steckel, 2011). But under some situations, even calculating correct HF equations is unable to estimate the bandgap properly for one type of semiconductors with strong electron correlations, i.e., Mott insulators (Cococcioni, 2012; Himmetoglu et al., 2014). Ongoing research efforts have been devoted to calculating more precise functionals through correcting procedures or alternatives to the density functionals. The use of these alternatives and corrections largely depends on the character of the system in question, its size and complexity, and the expense required from the computer. One of the correction processes that are used to address the DFT electronic bandgap problem is the method of DFT+*U* correction that this chapter discusses. For all other approaches, such as the post-Hartree-Fock methods and the hybrid functionals, DFT+*U* correction has been demonstrated to be just as good as the other methods but with the extra large advantage of low computing expense. Through the appropriate correction of the electronic structure of the system of interest through the application of the *U* correction, other precise predictions of the intermolecular interactions and formation energies are achievable (Cococcioni, 2012). Moreover, the *U* correction will also improve the description of the physical feature, besides the electronic structure, such as the magnetic and structural characteristics of

correlated systems, the electron transfer energetics, and chemical reactions (Tolba et al., 2018). Still, one of the drawbacks of the Hubbard method is that it cannot predict the properties of systems with more delocalized electrons, for example, metals. The relative effectiveness of the DFT+*U* method stems from its direct method in fixing the underestimated electronic interactions by merely adding a semiempirically adjusted numerical parameter "*U*" (Himmetoglu et al., 2014). The interaction value is easily adjustable, thus making the DFT+U method a method for providing a qualitative estimate of the electronic correlations' effect on a system's physical properties (Tolba et al., 2018).

2.8 COMPUTATIONAL APPROACH

The *ab initio* computations covered here were carried out with the plane wave Quantum-ESPRESSO simulation package (Giannozzi et al., 2009), which is based on density functional theory (DFT). Ultrasoft pseudopotentials were applied to the core electrons (Vanderbilt, 1990). For converged results, a plane-wave energy cutoff of 50 Ryd was employed, which was adequate. The PBEsol exchange-correlation functional was used because it is very helpful for computing structural data (Perdew et al., 1996, 2008) and enhances the prediction of solids' structural properties (Blanca Romero et al., 2014; Dongho Nguimdo & Joubert, 2015; Perdew et al., 2008). Convergence conditions for the structural optimisation were $10^{-5}R_y$ for total energy and $10^{-4}\,{}^{R_y}/_{a_0}$ for force, where a_0 is the Bohr radius. The diagonalisation approach developed by (Davidson, 1975) was applied. Although this depends on the structure, the average number of iteration steps required to obtain convergence was less than 50 for single point computations and less than 30 for geometry optimisation.

The DFT+U computations included Hubbard U parameters derived from fundamental principles using the linear response approach proposed by (Cococcioni & De Gironcoli, 2005). This method, which has also been used in earlier investigations, calculates U parameter values by tracking changes in d-state occupancy as a function of an applied perturbing potential. The Poormanwannier.x tool, which is part of the Quantum-ESPRESSO package, was used to create the Wannier functions-based representation of the 3d orbitals and count the occupancy of d states. This Wannierization approach is used to better describe the electrical structure of the DFT+U framework. The results generated with this method are known as DFT+U(WF) (Ting & Kowalski, 2023).

2.8 The Hubbard *U* Parameter

2.8.1 Origin of the Self-Interaction Error (SIE) in DFT

Standard density functional theory (DFT), including local-density (LDA) and generalised-gradient (GGA) approximations, suffers from self-interaction errors (SIE) when an electron interacts with itself. This leads to over-delocalisation of localised electrons—such as transition metal d or f states—and erroneous predictions such as metallic ground states for materials that are experimentally insulating (Himmetoglu & Janotti, 2016; Timrov et al., 2018). These inaccuracies also result in underestimated band gaps and erroneous magnetic properties.

2.8.2 Introduction of the DFT + *U* Method

To fix SIE, the DFT+*U* method introduces an on-site Coulomb penalty (*U*), energetically penalising the fractional occupation of local d or f orbitals, and localisation is restored at low expense relative to improved methods (Timrov et al., 2018, 2021). Most widely used, perhaps, is a rotationally invariant implementation (Anisimov et al., 1991, 1997; Dudarev et al., 1998), for which the DFT total energy correction is:

$$E_{DFT+U} = E_{DFT} + \frac{1}{2}\sum_{I\sigma} U^{I}\mathrm{Tr}[(1 - n^{I\sigma})n^{I\sigma}],$$

Here, $U^{I} = U - J$ is the effective on-site Coulomb interaction (Hubbard *U* minus Hund's exchange J), and $n^{I\sigma}$ are occupation matrices from projectors onto localised atomic orbitals [Eq. (2)]. The subsequent Hubbard potential V^{Hub}, obtained from the functional differentiation of E_U, acts selectively on these localised states, which helps in improving the depiction of correlation effects in systems such as transition-metal oxides (Cococcioni & De Gironcoli, 2005; Dabo et al., 2010; Kulik et al., 2006).

2.8.3 Methods of Choosing the Hubbard *U* Value

It is very important to choose an important *U* value. It can be computed *ab initio*—for example, using the constrained RPA (Alameda et al., 2017) or linear-response constrained DFT—or fitted semiempirically to reproduce bulk properties such as lattice constants, band gaps, or magnetic moments (Bhaskar et al., 2021; Bury et al., 2023; B. Zhang et al., 2020). Bulk-optimised *U* values, however, might not lead to valid conclusions for surfaces or interfaces, where local coordination, oxidation states, and adsorbate interactions may profoundly affect screening effects.

2.8.4 How to calculate U: LR-cDFT

In the standard linear-response constrained DFT (LR-cDFT) method (Cococcioni & De Gironcoli, 2005), *U* is calculated by perturbing the potential of chosen atoms and taking measurements of the electronic response:

$U^I = (\chi_0^{-1} - \chi^{-1})_{II}$,

Where χ and χ_o are the non-interacting and interacting response matrices, respectively. Even though the LR-cDFT is accurate, it is computationally demanding owing to finite-difference derivatives and supercell demands and poorly scales with system size, which may introduce numerical noise (Timrov et al., 2018).

2.8.5 Improved computation with DFPT

To address the limitations of LR-cDFT, Timrov et al. (2018) reinvented U computation using density-functional perturbation theory (DFPT). The method substitutes monochromatic perturbations in reciprocal space for supercell finite differences, enabling calculations within the primitive unit cell. DFPT provides:

• High accuracy by bypassing numerical differentiation
• Linear scaling with the number of perturbations
• Improved automation and symmetry handling
• Lower processing expense than LR-cDFT

2.8.6 Non-Universality of *U* and System-Specific Dependence

An important inference from computational as well as experimental studies is that *U* is not a universal constant for a given material or element. It changes with the oxidation state, local geometry, and the parameters that characterise the Hubbard manifold (Timrov et al., 2018). It is thus often necessary to perform surface-specific benchmarking or environment-dependent calculations to provide accurate estimates of surface chemistry, adsorption energetics, and redox activity.

2.9 QUANTUM ESPRESSO

The Quantum ESPRESSO (QE) suite is an integrated collection of open-source computer programs for electronic-structure calculations and materials modelling based on density-functional theory (DFT), plane-wave basis sets, and pseudopotentials (norm-conserving, ultrasoft, and projector-augmented wave) (Giannozzi et al., 2009). It is mainly used in material science research, and it is optimised for parallel processing

QE uses methods for solving Kohn–Sham equations, structural relaxations, ab initio molecular dynamics, calculations of phonons by density-functional perturbation theory, and calculation of properties such as electronic density of states, charge densities, and magnetic properties (Becke, 1993a; Dreizler & Gross, 1990; Parr & Yang, 1989; Perdew et al., 1992; Perdew, Ernzerhof, et al., 1996; Pickett, 1989; Stephens et al., 1994; Tao et al., 2003).

For this work, the primary components used are PWscf, PostProc, and Poormanwannier tools:

• PWscf performs self-consistent field (SCF) calculations using iterative diagonalisation within the plane-wave pseudopotential framework, supports LDA, GGA, and advanced functionals (e.g., Hubbard U, hybrid functionals), and allows structural optimisation and Brillouin zone sampling using various smearing techniques (Becke, 1993a; Blöchl, 1994; Gebauer & Baroni, 2000; Henkelman & Jónsson, 1999; Mermin, 1965; Methfessel & Paxton, 1989; Oda et al., 1998; Perdew, Ernzerhof, et al., 1996; Stephens et al., 1994; Tao et al., 2003).

• PostProc enables examination of QE output, including charge and spin densities, projected DOS, STM pictures, and provides interfaces to programs like pw2wannier90 for tight-binding models (Baldereschi et al., 1988; Tersoff & Hamann, 1985).

• Poormanwannier computes maximally localised Wannier functions based on QE wavefunctions and generates tight-binding Hamiltonians for band structure interpolation and investigation of transport and other Fermi surface-related features (Marzari & Vanderbilt, 1997; Mostofi et al., 2008; Souza et al., 2001; Yates et al., 2007).

The defined methods and tools above lay down the framework for the modelling and studying structural and electrical properties of materials that are relevant to this work

CONCLUSION

Overall, Chapter 2 laid out the methodology framework of the current study through the combination of DFT and Hubbard *U* corrections in order to extend DFT calculations to treat correlation effects in transition-metal chlorides. Such systematic methodology allows both binary and multi-component systems to be investigated, while garnering significant

new insights into the effects of entropy and electron localisation. These computational approaches then act as the foundation upon which the results and discussion in Chapter 3 are based.

CHAPTER 3: RESULTS AND DISCUSSION

CHAPTER 3: RESULTS AND DISCUSSIONS

INTRODUCTION

The aims of this master's thesis are to provide reference data on the electronic structures of single- and multiple-TM high-entropy lithium chlorides, which, in the long-term perspective, could be used to understand the electrochemical performance of these compounds. The computation of density of states (DOS) represents the main analysis framework, providing information concerning band structure, spin polarisation, and giving a hint at the electronic conductivity of the materials. Some previous high-entropy oxide research indicated that the electronic conductivity, as well as the materials' stability, may be promoted due to the presence of configurational disorder (Bérardan et al., 2016; Sarkar et al., 2018). Although the latter aspect was much less investigated in halide systems.

This chapter starts with research on $\mathrm{Li_2Me^{2+}Cl_4}$ compounds with the fixed U and different U parameters, hence preparing the grounds for electronic and magnetic properties of the researched materials.

The discussion is then advanced to a multi-component high-entropy chloride, in which electronic state extension and electronic delocalisation are. Lastly, the study of the influence of element-dependent U parameters is discussed, shedding some light on the electron localisation and correlation effects. These parameters have been derived by Dr. Kowalski with the aid of the linear response method(Cococcioni & De Gironcoli, 2005).

We applied two computational schemes: Model 1, in which a constant Hubbard parameter U = 5 eV was assumed for all transition metals, while in Model 2, we employed variable values for the U parameter. The calculations were done for TMs in low and high spin states to see how the spin arrangement affects the DOSes. We used the Quantum Espresso (QE) package to do the DFT calculations, and Xmgrace software to plot the DOS vs Energy.

Model 1: U = 5 eV

Model 1 used a fixed Hubbard parameter of U = 5 eV for Me^{2+} (Fe, Co, Mn, and Zn) cations in $Li_2[Me^{2+}]Cl_4$. The results we obtained are going to serve as a reference data for comparing electronic behaviours between single and multi-component phase materials.

Analysis of Electronic Characteristics with Fixed *U* Parameter Values

1. Binary Compounds (Li_2FeCl_4, Li_2MnCl_4, Li_2CoCl_4, Li_2ZnCl_4, Li_2MgCl_4)

$\boldsymbol{Li_2FeCl_4}$ and $\boldsymbol{Li_2CoCl_4}$ as shown in Figures 3.1.(1), 3.1.(3), 3.2.(1), and 3.2.(3) these compounds are computed as ferromagnetic, as evidenced by the asymmetry of the spin-up and spin-down DOS plots of *d* bands. Valence bands consist mainly of Cl(p) and transition metal (Co or Fe) *d*-bands. Of significance is the significant contribution from Fe(d) states above the Fermi level. The distance between the occupied and unoccupied states is about 4.

$\boldsymbol{Li_2MnCl_4}$ as shown in Figure 3.1.(2) and 3.2.(2), similar to the cobalt and iron compounds, Li_2MnC_4also shows a clear spin-polarised DOS. The occupied states below the Fermi level include large contributions from Mn(d) and Cl(p) orbitals, while the unoccupied conduction band is dominated by Mn(d) states. This material also has a similarly large band gap.

$\boldsymbol{Li_2ZnCl_4}$ The valence band is primarily formed of Cl(p) orbitals, and the significant contribution from Zn(d) orbitals is at much smaller energies, in the -6 to -7 eV range. This reveals that Li_2ZnCl_4 is an insulator with its band gap determined solely by Cl(p) states.

2. Electronic Structure of High-Entropy Compounds $Li_2(CoFeMnMgZn)Cl_4$

Finally, Figures 3.1.(5), 3.1.(6), and 3.1.(7) display the DOS of the CoFeMn multi-component system. The model structure was constructed by Dr. Kowalski based on experimental data measured at IET-1 institute at Forschungszentrum Jülich. Compared to the single-component cases, the multi-component DOS shows significant broadening of states and stronger hybridisation between p and d orbitals. This is a manifestation of entropy stabilisation, a characteristic feature of high-entropy systems that enhances electrons delocalisation and overall stability of the electronic structure.

Adding several transition metals (Co, Fe, Mg, Mn, Zn) to a single lattice site led to the formation of a high-entropy material, and DOS plots show a resulting complex electronic structure.

Valence Band Region: In all the high-entropy compositions, the valence band is predominantly formed of Cl(p) orbitals (green line), like in the binary compounds. But d-orbital contributions from every transition metal (Co, Fe, Mn, Zn) are observed at various energy levels, forming a more spread and hybridised valence band, but with the positions of individual TM *d* bands consistent with those obtained for single TM compounds. The contribution of Mg(p) orbitals is also observed, but less significantly.

Fermi Level and Conduction Band: The most striking feature is the significant contribution of the Fe *d* states at the edge of the valence band facing the Fermi level. This indicates that

out of the different considered elements, Fe should be the most active regarding the electrochemical performance of the material as well as the stabilisation of the structure. This is consistent with the first experimental data collected at the European Synchrotron Research Facility in Grenoble, France, by the host groups at Forschungszentrum Jülich.

(1)

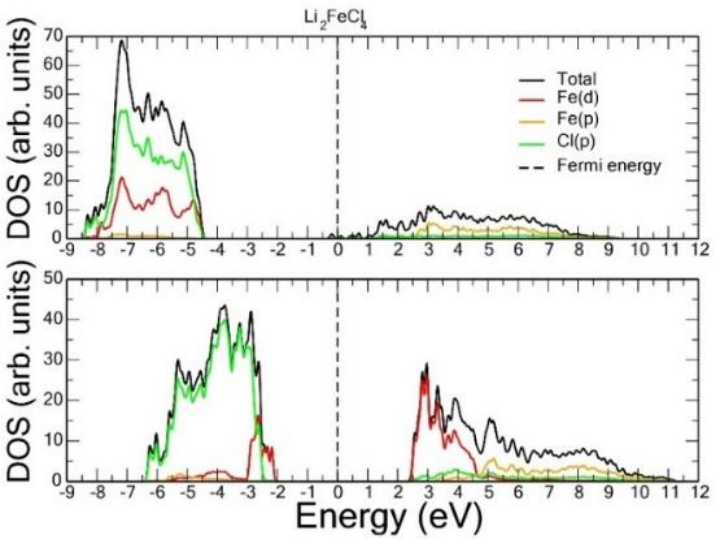

(2)

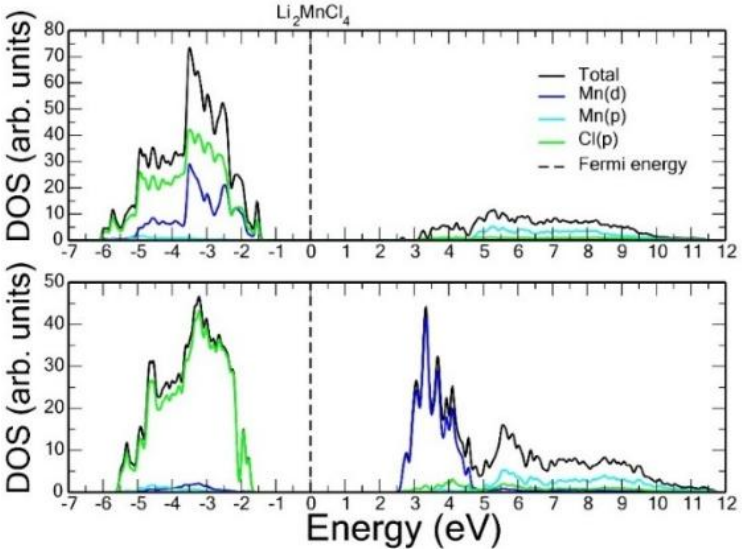

(3)

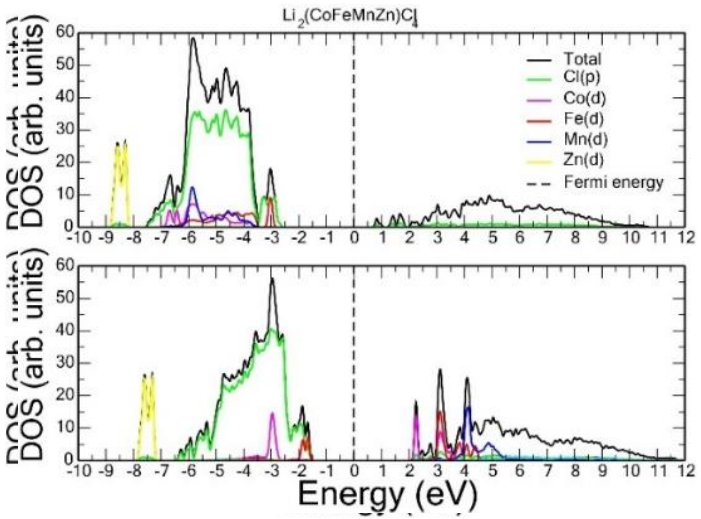
Li2(CoFeMnZn)Cl4
Total
Cl(p)
Co(d)
Fe(d)
Mn(d)
Zn(d)
Fermi energy
DOS (arb. units)
Energy (eV)

(4)

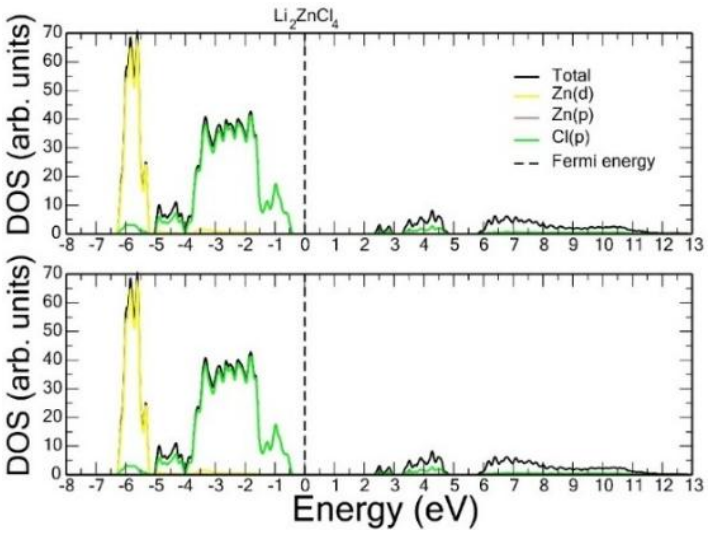
Li2ZnCl4
Total
Zn(d)
Zn(p)
Cl(p)
Fermi energy
DOS (arb. units)
Energy (eV)

(5)

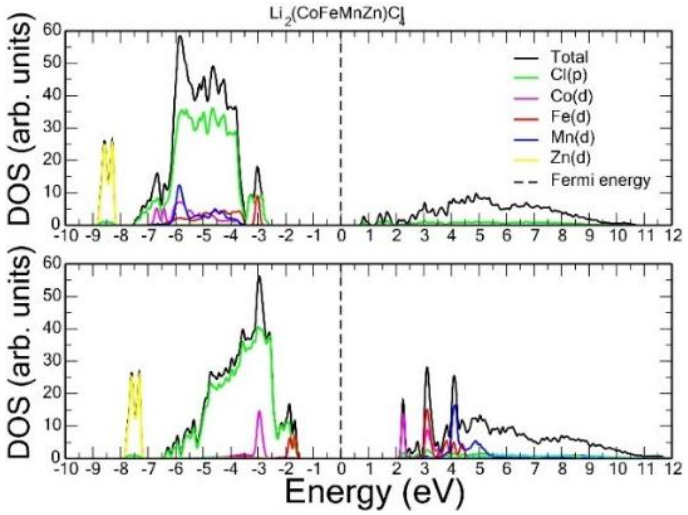
Li2(CoFeMnZn)Cl4
Total
Cl(p)
Co(d)
Fe(d)
Mn(d)
Zn(d)
Fermi energy
DOS (arb. units)
Energy (eV)

(6)

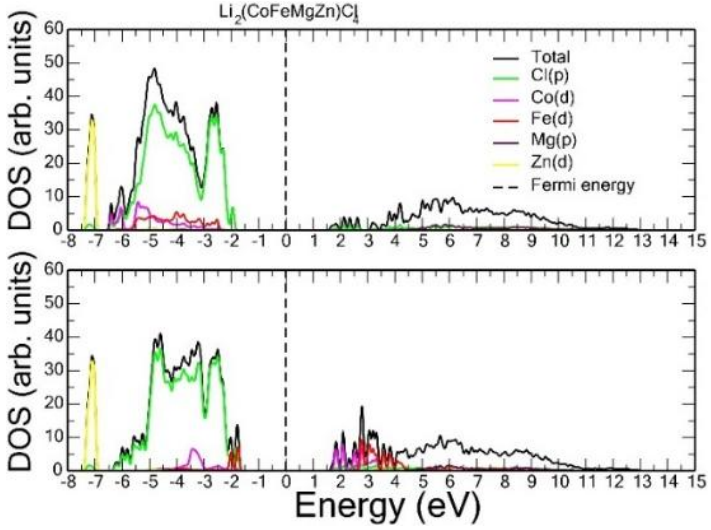
Li2(CoFeMgZn)Cl4
Total
Cl(p)
Co(d)
Fe(d)
Mg(p)
Zn(d)
Fermi energy
DOS (arb. units)
Energy (eV)

(7)

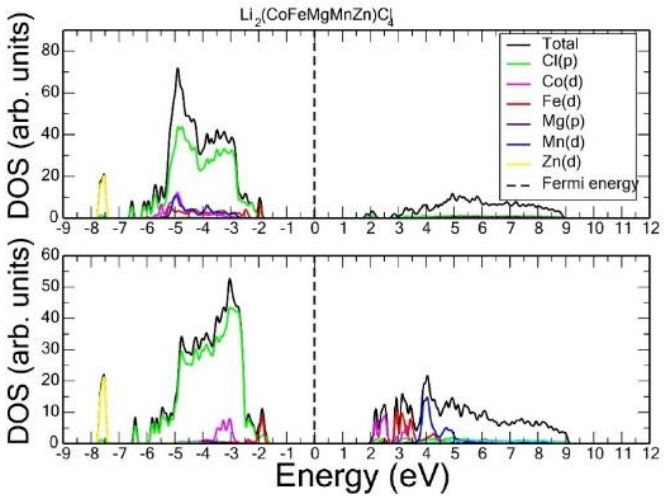

Figure 3.1: Single-phase and multi-phase (computed in High Spin) for various plots of the Density of States (DOS) as a function of Energy

Table 1: Electronic properties of binary and multi $Li_2[Me^{2+}]Cl_4$ compounds (computed in High Spin) at fixed Hubbard U = 5 eV

Compound	Redox State (Me^{2+})	Hubbard U (eV)	Spin States	Fermi energy ↑ (eV)	Fermi energy ↓ (eV)	Total energy (Ry)
Li_2FeCl_4	Fe(II)	5	High Spin	5.240	5.240	-3281.334
Li_2MnCl_4	Mn(II)	5	High Spin	5.227	5.227	-2091.150
Li_2CoCl_4	Co(II)	5	High Spin	4.909	3.256	-3624.046
Li_2ZnCl_4	Zn(II)	5	-	2.607	2.607	-4913.157
Li_2MgCl_4	Mg(II)	0	-	2.824	2.824	-1520.502
$Li_2(CoFeMnZn)Cl_4$	+2	5		2.388	2.388	-3688.299
$Li_2(CoFeMgZn)Cl_4$	+2	5		4.026	4.026	-3334.692
$Li_2(CoFeMnMgZn)Cl_4$	+2	5		3.169	3.169	-3265.569

(1)

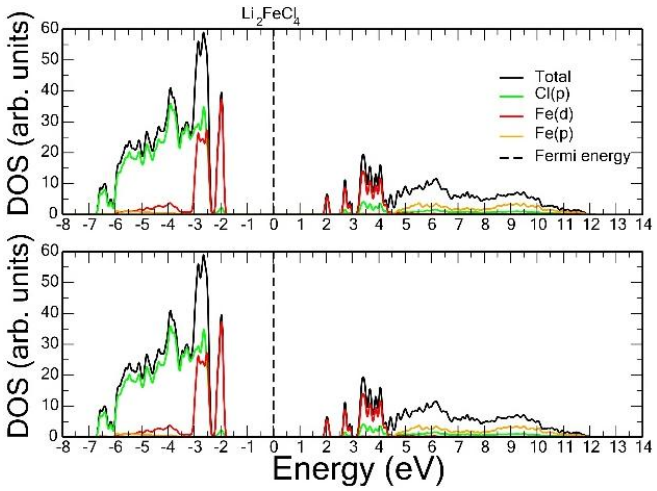
Li2FeCl4
DOS (arb. units)
Total
Cl(p)
Fe(d)
Fe(p)
Fermi energy
Energy (eV)

(2)

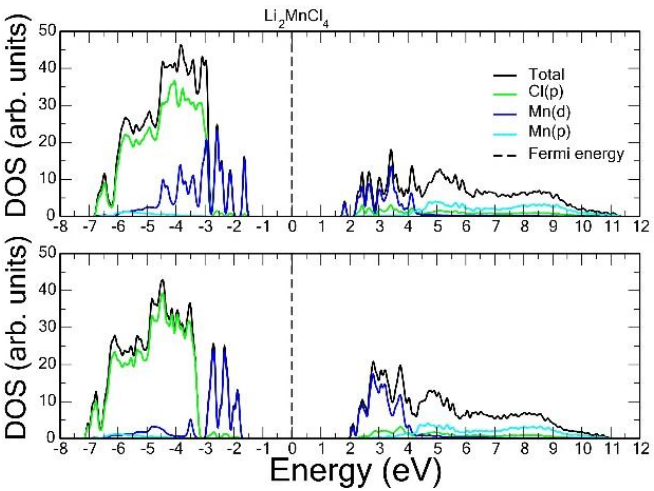
Li2MnCl4
DOS (arb. units)
Total
Cl(p)
Mn(d)
Mn(p)
Fermi energy
Energy (eV)

(3)

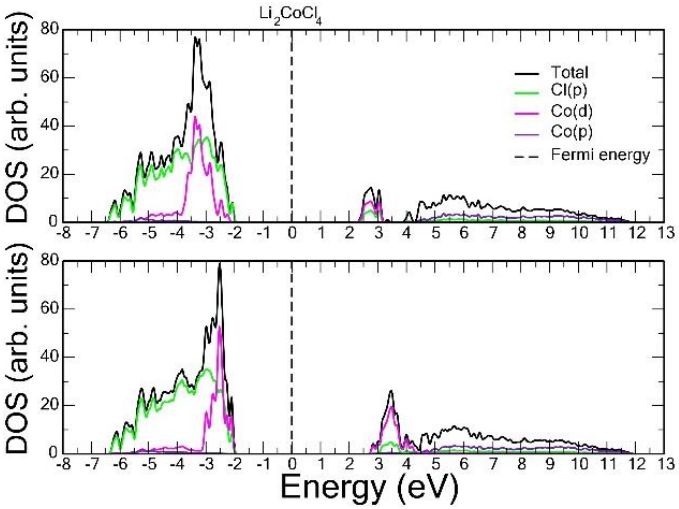
Li2CoCl4
DOS (arb. units)
Total
Cl(p)
Co(d)
Co(p)
Fermi energy
Energy (eV)

Figure 3.2: Single-phase and multi-phase (computed in Low Spin) for various plots of the Density of States (DOS) as a function of Energy

Table 2 : Electronic properties of binary $Li_2[Me^{2+}]Cl_4$ compounds (computed in Low Spin) at fixed Hubbard U = 5 eV

Compound	Redox State (Me^{2+})	Hubbard U (eV)	Spin States	Fermi energy ↑ (eV)	Fermi energy ↓ (eV)	Total energy (Ry)
Li_2FeCl_4	Fe(II)	5	Low Spin	4.073	4.0731	-3280.171
Li_2MnCl_4	Mn(II)	5	Low Spin	4.036	5.3987	-2938.874
Li_2CoCl_4	Co(II)	5	Low Spin	3.776	4.5746	-3623.503

Model 2: Variable U values

For Model 2, TM element-specific *U* values were used specifically for each element in an attempt to capture electronic correlation effects more accurately: Fe (5.5 eV), Mn (2.6 eV), Co (6 eV), Zn (5 eV), and Mg (0 eV). This enables a superior representation of electronic environments for each particular cation separately.

Analysis of Electronic Characteristics with Varying U Values

1. Binary Compounds (Li_2FeCl_4, Li_2MnCl_4, Li_2CoCl_4, Li_2ZnCl_4, Li_2MgCl_4)

$\boldsymbol{Li_2FeCl_4}$ and $\boldsymbol{Li_2CoCl_4}$ As shown in Figures 3.3.(1), 3.3.(3), and 3.4.(1) in these compounds, it is possible to distinguish in a clear-cut manner between spin-up and spin-down channels. The valence bands consist largely of the bands formed from Cl(p) states, while significant contributions are made by the transition metal d-states (Co/Fe) at lower energies of the valence band. The conduction bands are primarily described by the unoccupied d-states of Co and Fe, respectively. Adjustment of the *U* value appears to affect the location of the d-bands, with the possible consequence of giving a more accurate description of the electronic band gap.

Figure 3.3.(1) depicts the DOS of Fe(II) in optimised *U*, in which a deeper localisation in d-states is found in comparison to Module 1. Figure 3.3.(2) and 3.4.(1) shows the DOS for Co(II), with strong d-states splitting and a sharper, more localised DOS, in line with a larger value for *U* being used.

$\boldsymbol{Li_2MnCl_4}$ As shown in Figures 3.3.(2) and 3.4.(2), these compounds possess strong spin polarisation. The spin-up valence band consists mainly of Cl(p) states and occupied Mn(d) states. Meanwhile, the spin-down conduction band is characterised by the appearance of empty Mn(d) states. The role of the *U* parameter value is especially noticeable in such a situation, for it essentially separates the filled and empty d-states, thus potentially widening the band gap being estimated.

$\boldsymbol{Li_2ZnCl_4}$ as shown in Figure 3.3.(4), since it is a non-magnetic compound with a completely filled *d*-shell Zn^{2+}it doesn't show a large variation in its density of states (DOS) while imposing a U value. Zn(d) state band lies well within the valence band, i.e., at -6 eV, without spin polarisation. DOS remains spin channel symmetric all over and thus confirms its non-magnetic character. It has a clear band gap at the Fermi energy, further categorising it as an insulator or wide-bandgap semiconductor.

3. **High-Entropy Compound** ($\boldsymbol{Li_2(CoFeMnMgZn)Cl_4}$)

High-entropy alloy, $Li_2(CoFeMnMgZn)Cl_4$, has its electronic structure as a complicated merging of electronic properties inherent to its constituent element bases.

Valence Band: The valence band consists mainly of the Cl(p) states, albeit with

contributions in higher energies from d-states of Mn, Fe, and Co, in conjunction with Zn(d) states at low energies (approximately -7 eV). Contributing to it are Mg(p) orbitals to a lesser extent. The variation of *U* values for each of these transition metal systems of Co, Fe, and Mn provides a more complicated electronic structure such that their own *d*-states are shifted accordingly with the applied *U* value. It is with such variation that higher-order and wider density of states (DOS) features are realised than those derived for calculations from a single U value.

Conduction Band and Magnetism: The spin-down channel shows distinct peaks from the unoccupied d-states of Mn, Fe, and Co in the conduction band, whereas the spin-up channel has its states filled in the valence band. This spin difference makes the material show ferrimagnetic or ferromagnetic properties with a net magnetic moment. The specific Hubbard *U* parameter values play a role in giving a better estimate of these d-states' location and hybridisation, something that is critical for understanding electronic and magnetic properties of such complex disordered systems.

Table 3: Electronic properties of binary $Li_2[Me^{2+}]Cl_4$ compounds (computed in High Spin) with element-specific Hubbard U values

Compound	Redox State (Me^{2+})	Hubbard U (eV)	Spin States	Fermi energy ↑ (eV)	Fermi energy ↓ (eV)	Total energy (Ry)
Li_2FeCl_4	Fe(II)	5.5	High Spin	5.237	5.237	-3281.278
Li_2MnCl_4	Mn(II)	2.6	High Spin	5.232	5.232	-2940.930
Li_2CoCl_4	Co(II)	6	High Spin	4.908	4.908	-3623.948
Li_2ZnCl_4	Zn(II)	5	-	2.570	2.570	-4913.157
Li_2MgCl_4	Mg(II)	0	-	2.824	2.824	-1520.502

(1)

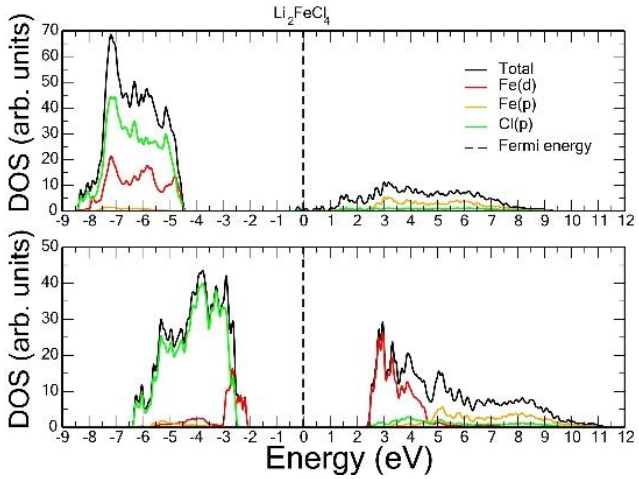
Li2FeCl4
DOS (arb. units)
DOS (arb. units)
Total
Fe(d)
Fe(p)
Cl(p)
Fermi energy
Energy (eV)

(2)

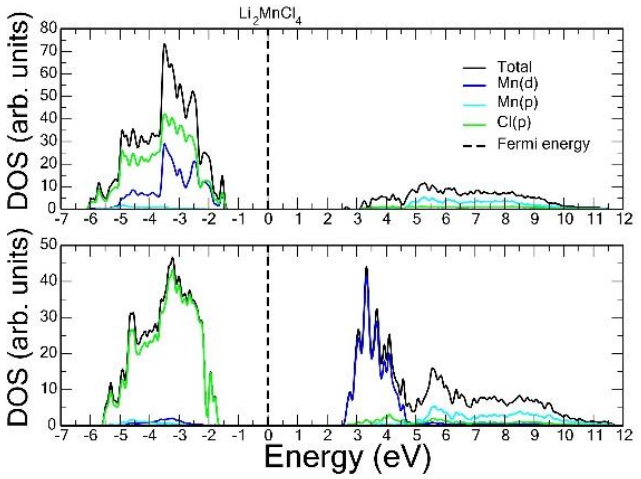
Li2MnCl4
DOS (arb. units)
DOS (arb. units)
Total
Mn(d)
Mn(p)
Cl(p)
Fermi energy
Energy (eV)

(3)

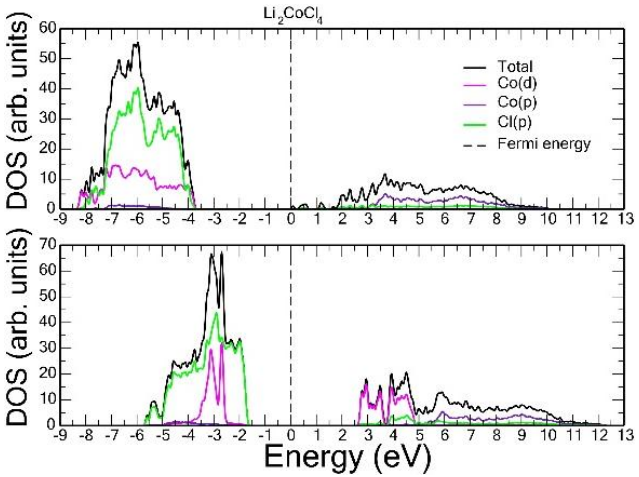
Li2CoCl4
DOS (arb. units)
DOS (arb. units)
Total
Co(d)
Co(p)
Cl(p)
Fermi energy
Energy (eV)

(4)

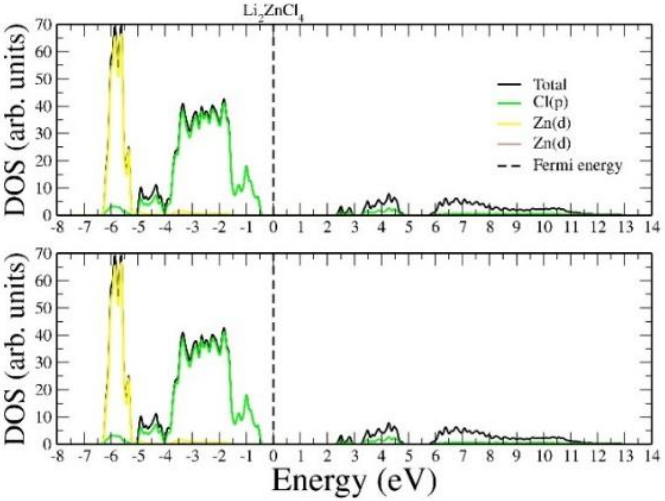
Li2ZnCl4
DOS (arb. units)
DOS (arb. units)
Total
Cl(p)
Zn(d)
Zn(d)
Fermi energy
Energy (eV)

(5)

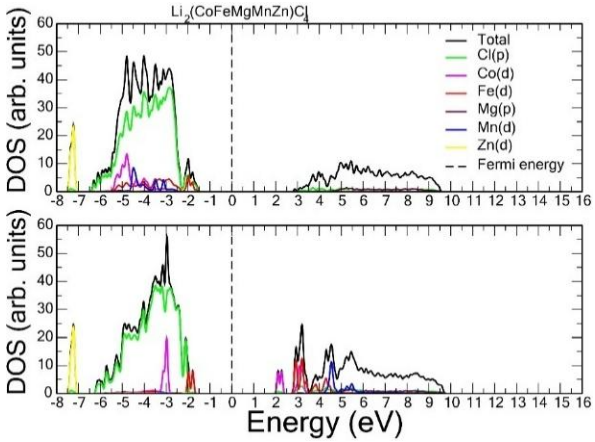

Figure 3.3: Single-phase and multi-phase (computed in High Spin) for various plots of the Density of States (DOS) as a function of Energy

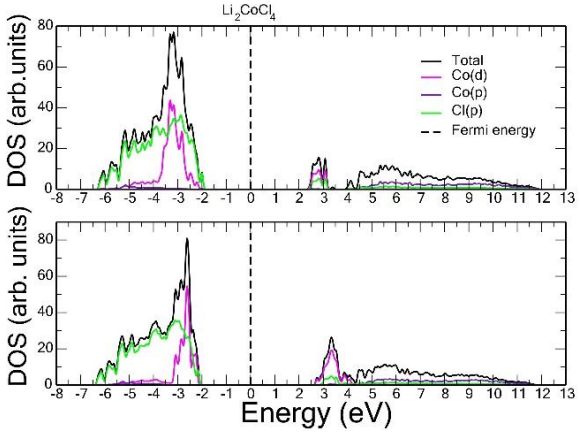

(2)

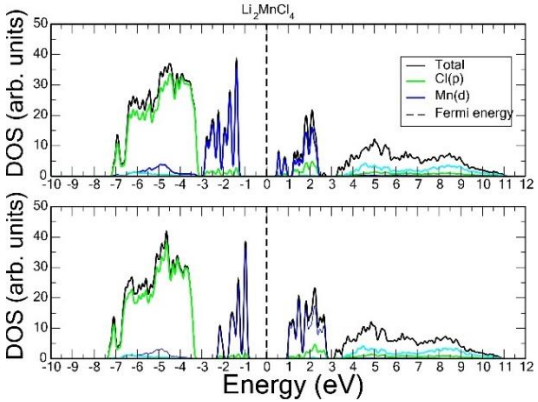

Figure 3.4: Single-phase and multi-phase (computed in Low Spin) for various plots of the Density of States (DOS) as a function of Energy

Table 4: Electronic properties of binary $Li_2[Me^{2+}]Cl_4$ compounds (computed in Low Spin) with element-specific Hubbard U values

Compound	Redox State (Me^{2+})	Hubbard U (eV)	Spin States	Fermi energy ↑ (eV)	Fermi energy ↓ (eV)	Total energy (Ry)
Li_2MnCl_4	Mn(II)	2.6	Low Spin	4.723	5.401	-2939.360
Li_2CoCl_4	Co(II)	6	Low Spin	3.774	4.573	-3623.327

The computed DOSes indicate that all compositions are wide band-gap insulators, with TMs d-bands contributing to the valence band at different energies. The most important observation is the contribution of the d-band of Fe, which happens to occur on the top of the valence band, making the compounds with Fe potentially electrochemically active. For the same reason, compounds with Fe should have larger electronic conductivity. We found that the value of the Hubbard U parameter itself does not significantly change the DOSes.

CONCLUSION

The key findings for this chapter are:

1. Fe, Mn, and Co have a significant contribution to the valence band, while Zn and Mg form a negligible contribution towards electronic conductivity. For Fe, spin state arrangements may play an additional role and this effect should be further investigated by computational or experimental methods.
2. The multi-component alloys (e.g., CoFeMn) have a large band gap, whiles the d orbital of Fe contributes to the top of the valence band
3. Although Model 2 with variable U values provides a more accurate description of the electronic structure, the general shape and position of DOSes are not significantly affected by the selection of the Hubbard *U* parameter.

CONCLUSION AND PERSPECTIVES

CONCLUSION AND PERSPECTIVES

CONCLUSION

Me^{2+} (Fe, Co, Mn, and Zn) cations in $Li_2[Me^{2+}]Cl_4$

This master's thesis has explored the electronic and ionic structures of certain high-entropy chlorides (HECls) as potential electrode materials (as a cathode material in lithium-ion batteries). Using density functional theory (DFT) in combination with the Quantum ESPRESSO computational suite, both constant and element-dependent Hubbard U corrections were applied to analyse the role of transition-metal d-orbitals in terms of electronic density of states (DOS) profiles, band structures, and spin polarisation of binary as well as multi-component compounds of the $\mathrm{Li_2[Me^{2+}]Cl_4}$ type, in which $Me^{2+}$is Fe, Mn, Co, Zn, and Mg.

Under this, the results show that binary chlorides show a range of electronic behaviours: Fe, Mn, and Co systems show insulating behaviour dominated by strong spin polarisation, while Zn and Mg systems act as non-magnetic insulators with large band gaps. In contrast, multi-component high-entropy chlorides show hybridised and broadened electronic states, with partially filled d-bands near the Fermi level. Such broadening due to disorder results in a semi-conducting or weakly insulating nature and highlights configurational entropy in stabilising hybridised electronic states, promoting orbital overlap, and assisting ion mobility.

Comparison of both calculation schemes demonstrated that although a non-uniform U of 5 eV is sufficient for robust qualitative insight, element-dependent U values give a finer characterisation of d-electron delocalisation and splitting effects. What is particularly important, both schemes result in convergent, mutually consistent conclusion: high-entropy chlorides demonstrate typical entropy-driven stability and electronic tunability with the potential of outperforming intrinsic shortcomings of traditional transition-metal oxide cathodes.

In summary, this work creates a calculation protocol and model data set that enables the interpretation and prediction of the electronic structures of high-entropy halide materials. The results offer useful guidance for current and future experimental verification by means of XANES and EXAFS at Forschungszentrum Jülich and collaborating laboratories. The results suggest Fe-based high-entropy chlorides as especially attractive cathode materials, offering configurational disorder along with desirable electronic properties.

This work facilitates the fundamental understanding of high-entropy chlorides, hence contributing to the grand scheme of developing low-cost, long-lasting, and high-efficiency

electrode materials. In this way, it clears a path to the realisation of future-generation lithium-ion batteries that will propel the global transition to sustainable energy infrastructure.

PERSPECTIVES

The DOSes computed in the scope of this master's thesis provide a basic understanding of the electronic structure of the $Li_2Me^{2+}Cl_4$ compounds. The obtained knowledge will serve as the reference for the follow-up analysis of the electronic structure of these compounds with different amounts of cation dopants and understanding of the XANES/EXAFS data collected by the experimental colleagues.

In order to fully understand the stability and electrochemical performance of these materials as cathodes for batteries, a thermodynamic evaluation is needed, including computation and/or potential measurements of thermodynamic parameters such as formation enthalpy and free energy. More thoughtful evaluation of the DOSes vs. measured synchrotron data should allow for better understanding of ionic structure formation in these materials and select a target composition with the best possible stability and electrochemical performance. Understanding of these complex materials requires a significant computational and experimental effort, and the results of this master's thesis are the first step towards understanding the performance of transition metal chlorides as materials for battery electrodes.

BIBLIOGRAPHIC REFERENCES

1. Aida, M. N. (2022). *A new spinel high-entropy oxides nanoparticles (FeCoNiMnZn) 3O4 as anode materials for lithium-ion batteries*. https://doi.org/10.58837/CHULA.THE.2022.261
2. Al-Gabalawy, M., Hosny, N. S., & Hussien, S. A. (2020). Lithium-ion battery modeling including degradation based on single-particle approximations. *Batteries*, *6*(3), 37.
3. Bérardan, D., Franger, S., Meena, A. K., & Dragoe, N. (2016). Room temperature lithium superionic conductivity in high entropy oxides. *Journal of Materials Chemistry A*, *4*(24), 9536–9541. https://doi.org/10.1039/c6ta03249d
4. Beridze, G., Birnie, A., Koniski, S., Ji, Y., & Kowalski, P. M. (2016). DFT+ U as a reliable method for efficient ab initio calculations of nuclear materials. *Progress in Nuclear Energy*, *92*, 142–146. https://doi.org/10.1016/j.pnucene.2016.07.012
5. Blanca Romero, A., Kowalski, P. M., Beridze, G., Schlenz, H., & Bosbach, D. (2014). Performance of DFT+U method for prediction of structural and thermodynamic parameters of monazite-type ceramics. *Journal of Computational Chemistry*, *35*(18), 1339–1346. https://doi.org/10.1002/jcc.23618
6. Blomgren, G. E. (2017). The Development and Future of Lithium Ion Batteries. *Journal of The Electrochemical Society*, *164*(1), A5019–A5025. https://doi.org/10.1149/2.0251701jes
7. Bresser, D., Passerini, S., & Scrosati, B. (2016). Leveraging valuable synergies by combining alloying and conversion for lithium-ion anodes. *Energy & Environmental Science*, *9*(11), 3348–3367. https://doi.org/10.1039/c6ee02346k
8. Cantor, B., Chang, I. T. H., Knight, P., & Vincent, A. J. B. (2004). Microstructural development in equiatomic multicomponent alloys. *Materials Science and Engineering: A*, *375–377*(1-2 SPEC. ISS.), 213–218. https://doi.org/10.1016/j.msea.2003.10.257
9. Chen, L., Wang, P., Shen, Y., & Guo, M. (2021). Spent lithium-ion battery materials recycling for catalytic pyrolysis or gasification of biomass. *Bioresource Technology*, *323*, 124584.

10. Chen, Y., Fu, H., Huang, Y., Huang, L., Zheng, X., Dai, Y., Huang, Y., & Luo, W. (2021). Opportunities for High-Entropy Materials in Rechargeable Batteries. *ACS Materials Letters*, *3*(2), 160–170. https://doi.org/10.1021/acsmaterialslett.0c00484
11. Chroneos, A., Rushton, M. J. D., Jiang, C., & Tsoukalas, L. H. (2013). Nuclear wasteform materials: Atomistic simulation case studies. *Journal of Nuclear Materials*, *441*(1), 29–39. https://doi.org/https://doi.org/10.1016/j.jnucmat.2013.05.012
12. Cococcioni, M., & De Gironcoli, S. (2005). Linear response approach to the calculation of the effective interaction parameters in the LDA+U method. *Physical Review B - Condensed Matter and Materials Physics*, *71*(3), 1–16. https://doi.org/10.1103/PhysRevB.71.035105
13. Connor, T., Cheong, O., Bornhake, T., Shad, A. C., Tesch, R., Sun, M., He, Z., Bukayemsky, A., Vinograd, V. L., Finkeldei, S. C., & Kowalski, P. M. (2021). Pyrochlore Compounds From Atomistic Simulations. *Frontiers in Chemistry*, *9*(November), 1–14. https://doi.org/10.3389/fchem.2021.733321
14. Davidson, E. R. (1975). The iterative calculation of a few of the lowest eigenvalues and corresponding eigenvectors of large real-symmetric matrices. *Journal of Computational Physics*, *17*(1), 87–94. https://doi.org/10.1016/0021-9991(75)90065-0
15. Dehghani-Sanij, A. R., Tharumalingam, E., Dusseault, M. B., & Fraser, R. (2019). Study of energy storage systems and environmental challenges of batteries. *Renewable and Sustainable Energy Reviews*, *104*, 192–208. https://doi.org/10.1016/j.rser.2019.01.023
16. Deng, D. (2015). Li-ion batteries: basics, progress, and challenges. *Energy Science & Engineering*, *3*(5), 385–418. https://doi.org/https://doi.org/10.1002/ese3.95
17. Dongho Nguimdo, G. M., & Joubert, D. P. (2015). A density functional (PBE, PBEsol, HSE06) study of the structural, electronic and optical properties of the ternary compounds AgAlX2 (X = S, Se, Te). *The European Physical Journal B*, *88*(5), 113. https://doi.org/10.1140/epjb/e2015-50478-x
18. Dunn, B., Kamath, H., & Tarascon, J. M. (2011). Electrical energy storage for the grid: A battery of choices. *Science*, *334*(6058), 928–935. https://doi.org/10.1126/science.1212741

19. Feng, J., Xiao, B., Zhou, R., & Pan, W. (2013). Anisotropy in elasticity and thermal conductivity of monazite-type REPO4 (RE = La, Ce, Nd, Sm, Eu and Gd) from first-principles calculations. *Acta Materialia*, *61*(19), 7364–7383. https://doi.org/10.1016/j.actamat.2013.08.043
20. Fergus, J. W. (2010). Recent developments in cathode materials for lithium ion batteries. *Journal of Power Sources*, *195*(4), 939–954. https://doi.org/10.1016/j.jpowsour.2009.08.089
21. Gallo, A. B., Simões-Moreira, J. R., Costa, H. K. M., Santos, M. M., & Moutinho dos Santos, E. (2016). Energy storage in the energy transition context: A technology review. *Renewable and Sustainable Energy Reviews*, *65*, 800–822. https://doi.org/10.1016/j.rser.2016.07.028
22. Gao, M. C., Liaw, P. K., Yeh, J. W., & Zhang, Y. (2016). High-entropy alloys: Fundamentals and applications. In *High-Entropy Alloys: Fundamentals and Applications*. https://doi.org/10.1007/978-3-319-27013-5
23. Garche, J. (2024). *Encyclopedia of electrochemical power sources*. Elsevier.
24. Giagloglou, K., Payne, J. L., Crouch, C., Gover, R. K. B., Connor, P. A., & Irvine, J. T. S. (2018). Transition Metal Chlorides NiCl 2 , KNiCl 3 , Li 6 VCl 8 and Li 2 MnCl 4 as Alternative Cathode Materials in Primary Li Thermal Batteries . *Journal of The Electrochemical Society*, *165*(14), A3510–A3516. https://doi.org/10.1149/2.1231814jes
25. Giannozzi, P., Baroni, S., Bonini, N., Calandra, M., Car, R., Cavazzoni, C., Ceresoli, D., Chiarotti, G. L., Cococcioni, M., Dabo, I., Dal Corso, A., De Gironcoli, S., Fabris, S., Fratesi, G., Gebauer, R., Gerstmann, U., Gougoussis, C., Kokalj, A., Lazzeri, M., … Wentzcovitch, R. M. (2009). QUANTUM ESPRESSO: A modular and open-source software project for quantum simulations of materials. *Journal of Physics Condensed Matter*, *21*(39), 395502. https://doi.org/10.1088/0953-8984/21/39/395502
26. Gong, Z., & Yang, Y. (2011). Recent advances in the research of polyanion-type cathode materials for Li-ion batteries. *Energy & Environmental Science*, *4*(9), 3223–3242. https://doi.org/10.1039/c0ee00713g
27. Grey, C. P., & Tarascon, J. M. (2016). Sustainability and in situ monitoring in battery development. *Nature Materials*, *16*(1), 45–56. https://doi.org/10.1038/nmat4777

28. Han, L., Liu, Y. M., Lu, W. Z., & Xiao, F. (2014). Design of Automatic Production Line for Electrode Defects Inspection of Li-Ion Power Battery. *Applied Mechanics and Materials*, *470*, 400–403. https://doi.org/10.4028/www.scientific.net/AMM.470.400
29. Hanson, E. D., Lilley, L. M., Cain, J. D., Hao, S., Palacios, E., Aydin, K., Wolverton, C., Meade, T., & Dravid, V. P. (2019). Phase engineering and optical properties of 2D MoSe2: Promise and pitfalls. *Materials Chemistry and Physics*, *225*, 219–226. https://doi.org/10.1016/j.matchemphys.2018.11.069
30. Hitz, E., Wan, J., Patel, A., Xu, Y., Meshi, L., Dai, J., Chen, Y., Lu, A., Davydov, A. V, & Hu, L. (2016). Electrochemical intercalation of lithium ions into NbSe2 nanosheets. *ACS Applied Materials & Interfaces*, *8*(18), 11390–11395. https://doi.org/10.1021/acsami.5b11583
31. Holgate, T. C., Liu, Y., Hitchcock, D., Tritt, T. M., & He, J. (2013). Thermoelectric Properties of Li-Intercalated ZrSe 2 Single Crystals. *Journal of Electronic Materials*, *42*, 1751–1755. https://doi.org/10.1007/s11664-012-2410-1
32. Holgate, T. C., Zhu, S., Zhou, M., Bangarigadu-Sanasy, S., Kleinke, H., He, J., & Tritt, T. M. (2013). Thermoelectric transport properties of polycrystalline titanium diselenide co-intercalated with nickel and titanium using spark plasma sintering. *Journal of Solid State Chemistry*, *197*, 273–278. https://doi.org/10.1016/j.jssc.2012.07.057
33. Hou, X., Liu, X., Wang, H., Zhang, X., Zhou, J., & Wang, M. (2023). Specific countermeasures to intrinsic capacity decline issues and future direction of LiMn2O4 cathode. *Energy Storage Materials*, *57*(December 2022), 577–606. https://doi.org/10.1016/j.ensm.2023.02.015
34. Hussain, I., Lamiel, C., Ahmad, M., Chen, Y., Shuang, S., Javed, M. S., Yang, Y., & Zhang, K. (2021). High entropy alloys as electrode material for supercapacitors: A review. *Journal of Energy Storage*, *44*(PA), 103405. https://doi.org/10.1016/j.est.2021.103405
35. Itoh, M., Inaguma, Y., Jung, W. H., Chen, L., & Nakamura, T. (1994). High lithium ion conductivity in the perovskite-type compounds Ln1 2Li1 2TiO3(Ln=La,Pr,Nd,Sm). *Solid State Ionics*, *70–71*(PART 1), 203–207. https://doi.org/10.1016/0167-2738(94)90310-7

36. Jahn, S., & Kowalski, P. M. (2014). Theoretical approaches to structure and spectroscopy of Earth materials. *Spectroscopic Methods in Mineralogy and Materials Sciences*, *78*, 691–743. https://doi.org/10.2138/rmg.2014.78.17
37. Ji, L., Lin, Z., Alcoutlabi, M., & Zhang, X. (2011). Recent developments in nanostructured anode materials for rechargeable lithium-ion batteries. *Energy & Environmental Science*, *4*(8), 2682–2699. https://doi.org/10.1039/c0ee00699h
38. Jiang, S., Hu, T., Gild, J., Zhou, N., Nie, J., Qin, M., Harrington, T., Vecchio, K., & Luo, J. (2018). A new class of high-entropy perovskite oxides. *Scripta Materialia*, *142*, 116–120. https://doi.org/10.1016/j.scriptamat.2017.08.040
39. Julien, C. M., Mauger, A., Zaghib, K., & Groult, H. (2014). Comparative issues of cathode materials for Li-ion batteries. *Inorganics*, *2*(1), 132–154. https://doi.org/10.3390/inorganics2010132
40. Kalair, A., Abas, N., Saleem, M. S., Kalair, A. R., & Khan, N. (2021). Role of energy storage systems in energy transition from fossil fuels to renewables. *Energy Storage*, *3*(1), 1–27. https://doi.org/10.1002/est2.135
41. Kalyani, P., & Kalaiselvi, N. (2005). Various aspects of LiNiO2 chemistry: A review. *Science and Technology of Advanced Materials*, *6*(6), 689–703. https://doi.org/10.1016/j.stam.2005.06.001
42. Kanno, R., Takeda, Y., & Yamamoto, O. (1981). Ionic conductivity of solid lithium ion conductors with the spinel structure: Li2MCl4 (M = Mg, Mn, Fe, Cd). *Materials Research Bulletin*, *16*(8), 999–1005. https://doi.org/10.1016/0025-5408(81)90142-2
43. Kim, T., Song, W., Son, D. Y., Ono, L. K., & Qi, Y. (2019). Lithium-ion batteries: outlook on present, future, and hybridized technologies. *Journal of Materials Chemistry A*, *7*(7), 2942–2964. https://doi.org/10.1039/C8TA10513H
44. Kokal, I., Somer, M., Notten, P. H. L., & Hintzen, H. T. (2011). Sol-gel synthesis and lithium ion conductivity of Li7La 3Zr2O12 with garnet-related type structure. *Solid State Ionics*, *185*(1), 42–46. https://doi.org/10.1016/j.ssi.2011.01.002
45. Koohi-Fayegh, S., & Rosen, M. A. (2020). A review of energy storage types, applications and recent developments. *Journal of Energy Storage*, *27*, 101047. https://doi.org/https://doi.org/10.1016/j.est.2019.101047

46. Kowalski, P. M., Bornhake, T., Cheong, O., Dohrmann, N., Koch Liston, A. L., Potts, S. K., Shad, A., Tesch, R., & Ting, Y.-Y. Y. (2023). Fundamentals of energy storage from first principles simulations: Challenges and opportunities. *Frontiers in Energy Research*, *10*, 1096190. https://doi.org/10.3389/fenrg.2022.1096190
47. Kühne, M., Börrnert, F., Fecher, S., Ghorbani-Asl, M., Biskupek, J., Samuelis, D., Krasheninnikov, A. V, Kaiser, U., & Smet, J. H. (2018). Reversible superdense ordering of lithium between two graphene sheets. *Nature*, *564*(7735), 234–239. https://doi.org/10.1038/s41586-018-0754-2
48. Kumar, P. J., Nishimura, K., Senna, M., Düvel, A., Heitjans, P., Kawaguchi, T., Sakamoto, N., Wakiya, N., & Suzuki, H. (2016). A novel low-temperature solid-state route for nanostructured cubic garnet Li7La3Zr2O12 and its application to Li-ion battery. *RSC Advances*, *6*(67), 62656–62667. https://doi.org/10.1039/c6ra09695f
49. Liang, Y., Zhao, C.-Z., Yuan, H., Chen, Y., Zhang, W., Huang, J.-Q., Yu, D., Liu, Y., Titirici, M.-M., Chueh, Y.-L., Yu, H., & Zhang, Q. (2019). A review of rechargeable batteries for portable electronic devices. *InfoMat*, *1*(1), 6–32. https://doi.org/https://doi.org/10.1002/inf2.12000
50. Liu, G., Yuan, X., Yang, Y., Tao, J., & Chi, Y. (2019). Three-dimensional hierarchical wreath-like Co 3 O 4 @ TiO 2 as an anode for lithium-ion batteries. *Journal of Alloys and Compounds*, *780*, 948–958. https://doi.org/10.1016/j.jallcom.2018.11.242
51. Liu, S., Xiong, L., & He, C. (2014). Long cycle life lithium ion battery with lithium nickel cobalt manganese oxide (NCM) cathode. *Journal of Power Sources*, *261*, 285–291. https://doi.org/https://doi.org/10.1016/j.jpowsour.2014.03.083
52. Liu, Z., Zhang, G., Pepas, J., Ma, Y., & Chen, H. (2024). Li2FeCl4 as a Cost-Effective and Durable Cathode for Solid-State Li-Ion Batteries. *ACS Energy Letters*, *9*(11), 5464–5470. https://doi.org/10.1021/acsenergylett.4c02376
53. Löffler, T., Ludwig, A., Rossmeisl, J., & Schuhmann, W. (2021). What Makes High-Entropy Alloys Exceptional Electrocatalysts? In *Angewandte Chemie - International Edition* (Vol. 60, Issue 52, pp. 26894–26903). https://doi.org/10.1002/anie.202109212
54. Lun, Z., Ouyang, B., Kwon, D. H., Ha, Y., Foley, E. E., Huang, T. Y., Cai, Z., Kim, H., Balasubramanian, M., Sun, Y., Huang, J., Tian, Y., Kim, H., McCloskey, B. D., Yang, W., Clément, R. J., Ji, H., & Ceder, G. (2021). Cation-disordered rocksalt-type high-

entropy cathodes for Li-ion batteries. *Nature Materials*, *20*(2), 214–221. https://doi.org/10.1038/s41563-020-00816-0

55. Ma, E., & Wu, X. (2019). Tailoring heterogeneities in high-entropy alloys to promote strength–ductility synergy. *Nature Communications*, *10*(1), 1–10. https://doi.org/10.1038/s41467-019-13311-1
56. Mao, A., Xiang, H. Z., Zhang, Z. G., Kuramoto, K., Zhang, H., & Jia, Y. (2020). A new class of spinel high-entropy oxides with controllable magnetic properties. *Journal of Magnetism and Magnetic Materials*, *497*(July 2019), 1–5. https://doi.org/10.1016/j.jmmm.2019.165884
57. Meena, A. K. (2021). *All Solid State Batteries For High Power Density Applications*. Université Paris-Saclay.
58. Mukai, K., Sugiyama, J., & Aoki, Y. (2010). Structural, magnetic, and electrochemical studies on lithium insertion materials LiNi1−xCoxO2 with 0≤x≤0.25. *Journal of Solid State Chemistry*, *183*(7), 1726–1732. https://doi.org/https://doi.org/10.1016/j.jssc.2010.05.019
59. Musicó, B. L., Gilbert, D., Ward, T. Z., Page, K., George, E., Yan, J., Mandrus, D., & Keppens, V. (2020). The emergent field of high entropy oxides: Design, prospects, challenges, and opportunities for tailoring material properties. *APL Materials*, *8*(4). https://doi.org/10.1063/5.0003149
60. Ohno, K., Esfarjani, K., & Kawazoe, Y. (2003). Computational Materials Science. In *Computational Materials Science* (Vol. 28, Issue 2). https://doi.org/10.1142/9789813225862_0001
61. Ouyang, B., & Zeng, Y. (2024). The rise of high-entropy battery materials. In *Nature Communications* (Vol. 15, Issue 1). Nature Research. https://doi.org/10.1038/s41467-024-45309-9
62. Payne, J. L., Giagloglou, K., Carins, G. M., Crouch, C. J., Percival, J. D., Smith, R. I., Gover, R. K. B., & Irvine, J. T. S. (2018). In-situ studies of high temperature thermal batteries: A perspective. *Frontiers in Energy Research*, *6*, 1–6. https://doi.org/10.3389/fenrg.2018.00121
63. Pender, J. P., Jha, G., Youn, D. H., Ziegler, J. M., Andoni, I., Choi, E. J., Heller, A., Dunn, B. S., Weiss, P. S., Penner, R. M., & Mullins, C. B. (2020). Electrode

Degradation in Lithium-Ion Batteries. *ACS Nano*, *14*(2), 1243–1295. https://doi.org/10.1021/acsnano.9b04365

64. Perdew, J. P., Burke, K., & Ernzerhof, M. (1996). Generalized gradient approximation made simple. *Physical Review Letters*, *77*(18), 3865. https://doi.org/https://doi.org/10.1103/PhysRevLett.77.3865
65. Perdew, J. P., Ruzsinszky, A., Csonka, G. I., Vydrov, O. A., Scuseria, G. E., Constantin, L. A., Zhou, X., & Burke, K. (2008). Restoring the density-gradient expansion for exchange in solids and surfaces. *Physical Review Letters*, *100*(13), 136406. https://doi.org/10.1103/PhysRevLett.100.136406
66. Price, C. J. (2023). *Ab Initio Study of Intercalated TMDCs and Their Superlattices* (Issue October). University of Exeter (United Kingdom).
67. Rost, C. M., Sachet, E., Borman, T., Moballegh, A., Dickey, E. C., Hou, D., Jones, J. L., Curtarolo, S., & Maria, J. P. (2015). Entropy-stabilized oxides. *Nature Communications*, *6*(1), 8485. https://doi.org/10.1038/ncomms9485
68. Rustad, J. R. (2012). Density functional calculations of the enthalpies of formation of rare-earth orthophosphates. *American Mineralogist*, *97*(5–6), 791–799. https://doi.org/10.2138/am.2012.3948
69. Sarkar, A., Breitung, B., & Hahn, H. (2020). High entropy oxides: The role of entropy, enthalpy and synergy. *Scripta Materialia*, *187*, 43–48. https://doi.org/10.1016/j.scriptamat.2020.05.019
70. Sarkar, A., Velasco, L., Wang, D., Wang, Q., Talasila, G., de Biasi, L., Kübel, C., Brezesinski, T., Bhattacharya, S. S., Hahn, H., & Breitung, B. (2018). High entropy oxides for reversible energy storage. *Nature Communications*, *9*(1). https://doi.org/10.1038/s41467-018-05774-5
71. Sato, M., Lu, L., & Nagai, H. (2020). *Lithium-ion Batteries: Thin Film for Energy Materials and Devices*. IntechOpen.
72. Saxena, S., Sanchez, G., & Pecht, M. (2017). Batteries in portable electronic devices: A user's perspective. *IEEE Industrial Electronics Magazine*, *11*(2), 35–44. https://doi.org/10.1109/MIE.2017.2688483
73. Schumacher, S., Alekseev, E. V, Yu, S., Tempel, H., & Eichel, R.-A. (2025). High-Entropy Halides for Intercalation Battery Electrode Materials. *ChemElectroChem*, *12*(9), e202400659. https://doi.org/https://doi.org/10.1002/celc.202400659

74. Shi, J.-L., Xiao, D.-D., Ge, M., Yu, X., Chu, Y., Huang, X., Zhang, X.-D., Yin, Y.-X., Yang, X.-Q., Guo, Y.-G., Gu, L., & Wan, L.-J. (2018). High-Capacity Cathode Material with High Voltage for Li-Ion Batteries. *Advanced Materials*, *30*(9), 1705575. https://doi.org/https://doi.org/10.1002/adma.201705575
75. Shkvarin, A. S., Titov, A. A., Merentsov, A. I., Shkvarina, E. G., Postnikov, M. S., Píš, I., Nappini, S., Agzamova, P. A., Volegov, A. S., & Titov, A. N. (2021). The crystal structure, chemical bonding, and magnetic properties of the intercalation compounds CrxZrTe2 (x= 0–0.3). *Materials Science and Engineering: B*, *270*, 115218. https://doi.org/10.1016/j.mseb.2021.115218
76. Smith, A. I., Wladkowski, H. V, Hecht, Z. H., She, Y., Kattel, S., Samarawickrama, P. I., Rich, S. R., Murphy, J. R., Tian, J., & Ackerman, J. F. (2020). Alkali metal intercalation and reduction of layered WO2Cl2. *Chemistry of Materials*, *32*(24), 10482–10488. https://doi.org/10.1021/acs.chemmater.0c03270
77. Soloveichik, G. L. (2011). Battery technologies for large-scale stationary energy storage. *Annual Review of Chemical and Biomolecular Engineering*, *2*, 503–527. https://doi.org/10.1146/annurev-chembioeng-061010-114116
78. Stamenkovic, V. R., Strmcnik, D., Lopes, P. P., & Markovic, N. M. (2016). Energy and fuels from electrochemical interfaces. *Nature Materials*, *16*(1), 57–69. https://doi.org/10.1038/nmat4738
79. Starner, T. E. (2003). Powerful change part 1: batteries and possible alternatives for the mobile market. *IEEE Pervasive Computing*, *2*(4), 86–88.
80. Szymanski, N. J., Nevatia, P., Bartel, C. J., Zeng, Y., & Ceder, G. (2023). Autonomous and dynamic precursor selection for solid-state materials synthesis. *Nature Communications*, *14*(1). https://doi.org/10.1038/s41467-023-42329-9
81. Tian, Y., Zeng, G., Rutt, A., Shi, T., Kim, H., Wang, J., Koettgen, J., Sun, Y., Ouyang, B., Chen, T., Lun, Z., Rong, Z., Persson, K., & Ceder, G. (2021). *Promises and Challenges of Next-Generation " Beyond Li-ion " Batteries for Electric Vehicles and Grid Decarbonization*. https://doi.org/10.1021/acs.chemrev.0c00767
82. Ting, Y. Y., & Kowalski, P. M. (2023). Refined DFT＋U method for computation of layered oxide cathode materials. *Electrochimica Acta*, *443*, 141912. https://doi.org/10.1016/j.electacta.2023.141912

83. Tollefson, J. (2008). *Car industry: charging up the future*. Nature Publishing Group UK London.
84. Van Der Ven, A., Bhattacharya, J., & Belak, A. A. (2013). Understanding Li diffusion in Li-intercalation compounds. *Accounts of Chemical Research*, *46*(5), 1216–1225. https://doi.org/10.1021/ar200329r
85. Vanderbilt, D. (1990). Soft self-consistent pseudopotentials in a generalized eigenvalue formalism. *Physical Review B*, *41*(11), 7892.
86. Vogiatzis, K. D., Polynski, M. V, Kirkland, J. K., Townsend, J., Hashemi, A., Liu, C., & Pidko, E. A. (2019). Computational Approach to Molecular Catalysis by 3d Transition Metals: Challenges and Opportunities. *Chemical Reviews*, *119*(4), 2453–2523. https://doi.org/10.1021/acs.chemrev.8b00361
87. Wang, A., Kadam, S., Li, H., Shi, S., & Qi, Y. (2018). Review on modeling of the anode solid electrolyte interphase (SEI) for lithium-ion batteries. *NPJ Computational Materials*, *4*(1), 15. https://doi.org/10.1038/s41524-018-0064-0
88. Wang, L., Li, J., Lu, G., Li, W., Tao, Q., Shi, C., Jin, H., Chen, G., & Wang, S. (2020). Fundamentals of Electrolytes for Solid-State Batteries: Challenges and Perspectives. *Frontiers in Materials*, *7*(July), 1–5. https://doi.org/10.3389/fmats.2020.00111
89. Wang, Q., Velasco, L., Breitung, B., & Presser, V. (2021). High-Entropy Energy Materials in the Age of Big Data: A Critical Guide to Next-Generation Synthesis and Applications. *Advanced Energy Materials*, *11*(47), 2102355. https://doi.org/https://doi.org/10.1002/aenm.202102355
90. Wang, T., Chen, H., Yang, Z., Liang, J., & Dai, S. (2020). High-Entropy Perovskite Fluorides: A New Platform for Oxygen Evolution Catalysis. *Journal of the American Chemical Society*, *142*(10), 4550–4554. https://doi.org/10.1021/jacs.9b12377
91. Wang, T., Fan, J., Do-Thanh, C., Suo, X., Yang, Z., Chen, H., Yuan, Y., Lyu, H., Yang, S., & Dai, S. (2021). Perovskite Oxide–Halide Solid Solutions: A Platform for Electrocatalysts. *Angewandte Chemie*, *133*(18), 10041–10046. https://doi.org/10.1002/ange.202101120
92. Wei, L., Tao, J., Yang, Y., Fan, X., Ran, X., Li, J., Lin, Y., & Huang, Z. (2020). Surface sulfidization of spinel LiNi0. 5Mn1. 5O4 cathode material for enhanced

electrochemical performance in lithium-ion batteries. *Chemical Engineering Journal*, *384*, 123268. https://doi.org/10.1016/j.cej.2019.123268

93. Wen, Z., Huang, S., Yang, X., & Lin, B. (2008). High rate electrode materials for lithium ion batteries. *Solid State Ionics*, *179*(27–32), 1800–1805. https://doi.org/10.1016/j.ssi.2008.03.036
94. Wu, X., Kang, F., Duan, W., & Li, J. (2019). Density functional theory calculations: A powerful tool to simulate and design high-performance energy storage and conversion materials. *Progress in Natural Science: Materials International*, *29*(3), 247–255. https://doi.org/https://doi.org/10.1016/j.pnsc.2019.04.003
95. Wu, Y. (2015). *Lithium-ion batteries: Fundamentals and Applications*. CRC press.
96. Xu, X., Du, Y., Wang, C., Guo, Y., Zou, J., Zhou, K., Zeng, Z., Liu, Y., & Li, L. (2020). High-entropy alloy nanoparticles on aligned electronspun carbon nanofibers for supercapacitors. *Journal of Alloys and Compounds*, *822*, 153642. https://doi.org/10.1016/j.jallcom.2020.153642
97. Yan, J., Wang, D., Zhang, X., Li, J., Du, Q., Liu, X., Zhang, J., & Qi, X. (2020). A high-entropy perovskite titanate lithium-ion battery anode. *Journal of Materials Science*, *55*(16), 6942–6951. https://doi.org/10.1007/s10853-020-04482-0
98. Yan, S., Luo, S., Yang, L., Feng, J., Li, P., Wang, Q., Zhang, Y., & Liu, X. (2022). Novel P2-type layered medium-entropy ceramics oxide as cathode material for sodium-ion batteries. *Journal of Advanced Ceramics*, *11*(1), 158–171. https://doi.org/10.1007/s40145-021-0524-8
99. Yao, Y., Dong, Q., Brozena, A., Luo, J., Miao, J., Chi, M., Wang, C., Kevrekidis, I. G., Ren, Z. J., Greeley, J., Wang, G., Anapolsky, A., & Hu, L. (2022). High-entropy nanoparticles: Synthesis-structureproperty relationships and data-driven discovery. *Science*, *376*(6589). https://doi.org/10.1126/science.abn3103
100. Yeh, J. W., Chen, S. K., Lin, S. J., Gan, J. Y., Chin, T. S., Shun, T. T., Tsau, C. H., & Chang, S. Y. (2004). Nanostructured high-entropy alloys with multiple principal elements: Novel alloy design concepts and outcomes. In *Advanced Engineering Materials* (Vol. 6, Issue 5, pp. 299–303). https://doi.org/10.1002/adem.200300567
101. Ying, T., Yu, T., Shiah, Y. S., Li, C., Li, J., Qi, Y., & Hosono, H. (2021). High-Entropy van der Waals Materials Formed from Mixed Metal Dichalcogenides,

Halides, and Phosphorus Trisulfides. *Journal of the American Chemical Society*, *143*(18), 7042–7049. https://doi.org/10.1021/jacs.1c01580

102. Zeng, Y., Ouyang, B., Liu, J., Byeon, Y. W., Cai, Z., Miara, L. J., Wang, Y., & Ceder, G. (2022). High-entropy mechanism to boost ionic conductivity. *Science*, *378*(6626), 1320–1324. https://doi.org/10.1126/science.abq1346

103. Zhang, C., Wei, Y. L., Cao, P. F., & Lin, M. C. (2018). Energy storage system: Current studies on batteries and power condition system. *Renewable and Sustainable Energy Reviews*, *82*, 3091–3106. https://doi.org/10.1016/j.rser.2017.10.030

104. Zhang, R. Z., & Reece, M. J. (2019). Review of high entropy ceramics: design, synthesis, structure and properties. *Journal of Materials Chemistry A*, *7*(39), 22148–22162. https://doi.org/10.1039/c9ta05698j

105. Zhang, T., Li, D., Tao, Z., & Chen, J. (2013). Understanding electrode materials of rechargeable lithium batteries via DFT calculations. *Progress in Natural Science: Materials International*, *23*(3), 256–272. https://doi.org/https://doi.org/10.1016/j.pnsc.2013.04.005

106. Zhang, Y., Zuo, T. T., Tang, Z., Gao, M. C., Dahmen, K. A., Liaw, P. K., & Lu, Z. P. (2014). Microstructures and properties of high-entropy alloys. *Progress in Materials Science*, *61*(September 2013), 1–93. https://doi.org/10.1016/j.pmatsci.2013.10.001

107. Zhou, S., Chen, W., Shi, J., Li, G., Pei, F., Liu, S., Ye, W., Xiao, L., Wang, M.-S., Wang, D., Qiao, Y., Huang, L., Xu, G.-L., Liao, H.-G., Chen, J.-F., Amine, K., & Sun, S.-G. (2022). Efficient diffusion of superdense lithium via atomic channels for dendrite-free lithium–metal batteries. *Energy & Environmental Science*, *15*(1), 196–205. https://doi.org/10.1039/D1EE02205A

108. Zhu, J., Wierzbicki, T., & Li, W. (2018). A review of safety-focused mechanical modeling of commercial lithium-ion batteries. *Journal of Power Sources*, *378*(December 2017), 153–168. https://doi.org/10.1016/j.jpowsour.2017.12.034